Air. Worl

ESSA RESEARCH LABORATORIES

Air Resources Laboratories
Silver Spring, Maryland
June 1969

Atmospheric Transport and Diffusion in the Planetary Boundary Layer

Technical Memorandum ERLTM-ARL 14

U.S. DEPARTMENT OF COMMERCE / ENVIRONMENTAL SCIENCE SERVICES ADMINISTRATION

ESSA RESEARCH LABORATORIES

AIR RESOURCES LABORATORIES

IMPORTANT NOTICE

Technical Memoranda are used to insure prompt dissemination of special studies which, though of interest to the scientific community, may not be ready for formal publication. Since these papers may later be published in a modified form to include more recent information or research results, abstracting, citing, or reproducing this paper in the open literature is not encouraged. Contact the author for additional information on the subject matter discussed in this Memorandum.

U.S. DEPARTMENT OF COMMERCE
Environmental Science Services Administration
Research Laboratories

ESSA Technical Memorandum ERLTM-ARL 14

ATMOSPHERIC TRANSPORT AND DIFFUSION IN THE PLANETARY BOUNDARY LAYER

I. Van der Hoven, Editor

Contributors

J. K. Angell
A. B. Bernstein
D. J. Bjorem
C. R. Dickson
G. A. Herbert
E. H. Markee
G. E. Start
D. H. Slade
L. L. Wendell

Semiannual Research Program Review
July - December 1968
U. S. Atomic Energy Commission

Air Resources Laboratory
Silver Spring, Maryland
June 1969

PREFACE

In accordance with the letter of agreement of July 15, 1968, with the U. S. Atomic Energy Commission, Division of Reactor Development and Technology, Environmental and Sanitary Engineering Branch, the Air Resources Laboratories have continued their study of atmospheric transport and diffusion in the planetary boundary layer, micrometeorology, diffusion climatology, and the application of this work to the disposal of radioactive waste gases into the atmosphere. The research is technically administered and supervised through the Air Resources Environmental Laboratory of the Air Resources Laboratories. The work is performed at the Air Resources Laboratories Headquarters in Silver Spring, Maryland, and at the Air Resources Idaho Falls Laboratory, National Reactor Testing Station, Idaho. Any inquiry on the research being performed should be directed to the editor, Isaac Van der Hoven, Chief, Air Resources Environmental Laboratory, Air Resources Laboratories, Environmental Science Services Administration, 8060 - 13th Street, Silver Spring, Maryland 20910.

TABLE OF CONTENTS

ATMOSPHERIC TRANSPORT AND DIFFUSION IN THE PLANETARY BOUNDARY LAYER

AIR RESOURCES LABORATORIES SEMIANNUAL RESEARCH PROGRAM REVIEW
FOR THE ENVIRONMENTAL AND SANITARY ENGINEERING BRANCH
DIVISION OF REACTOR DEVELOPMENT AND TECHNOLOGY
U. S. ATOMIC ENERGY COMMISSION

JULY - DECEMBER 1968

1.0 RESEARCH AT AIR RESOURCES LABORATORIES HEADQUARTERS, SILVER SPRING, MD.

1.1 Low Altitude Constant Volume Balloon (Tetroon) Trajectories

(This project is a joint effort by personnel of the Air Resources Laboratories in Silver Spring, Maryland, and field offices. Support is provided jointly by the Atomic Energy Commission and the Public Health Service.)

The 'dominant' period of air parcel oscillation in the vertical within the planetary boundary layer has been estimated from the peaks in vertical-velocity spectra derived from 40 tetroon flights in the vicinity of the 460-m BREN tower at the Nevada Test Site. The atmospheric lapse rate at mean tetroon height has been determined from the temperatures obtained at several levels on the tower. Figure 1 shows reasonably good agreement between the dominant period as a function of lapse rate so obtained, and the Brunt-Vaisala period (P) expressed as follows

$$P = 2\pi \left[\frac{T_o}{g(\gamma_p - \gamma)}\right]^{1/2}, \qquad (1)$$

where T_o is the absolute temperature of the environment, g is the acceleration of gravity, γ_p is the process lapse rate (usually assumed dry adiabatic, γ_d), and γ is the lapse rate. As a consequence, there is a tendency for the air parcel (Lagrangian) wavelength to be proportional to wind speed and lapse rate. Because of this simple association, the kinematics, and perhaps dynamics, of the planetary boundary layer would appear to be more amenable to analysis from the Lagrangian than the Eulerian (fixed-position) point of view. It is suggested that the significance of the elementary Brunt-Vaisala concept has neither been sufficiently recognized, nor its ramifications properly exploited.

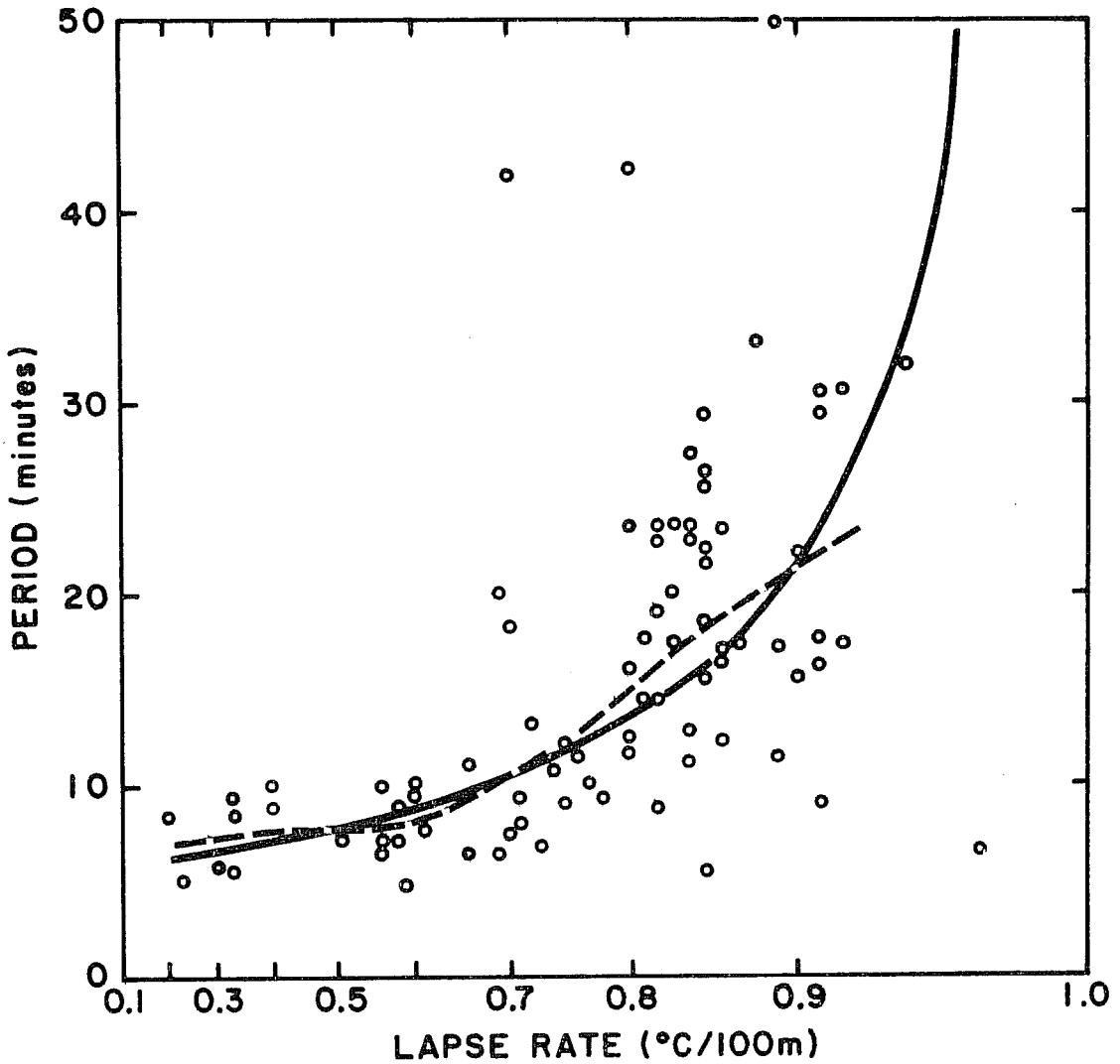

Figure 1. 'Dominant' period of tetroon oscillation in the vertical as a function of the lapse rate derived from BREN tower temperature measurements at the Nevada Test Site. The dashed line indicates the median period of tetroon oscillation in the vertical, the solid line represents the Brunt-Vaisala period in an unsaturated atmosphere. Note that the abscissa scale (lapse rate) is logarithmic.

Tetroon flights in the Bodega Bay area northwest of San Francisco have been used to determine the effect of a fairly sudden change in terrain height on the three-dimensional air motion. Figure 2 shows the average vertical-velocity field obtained by compositing by height the vertical velocities of 15 tetroon flights passing onshore in the early afternoon. The maximum upward motion (of magnitude 6 cm s^{-1}) occurs 250 m above the maximum in terrain slope; the sinking motion commencing 3 km inland may be associated with the decrease in terrain height and may also reflect the Brunt-Vaisala wavelength mentioned above. The sinking motion 400 m over the sea could indicate a highly modified form of a sea-breeze circulation regime. The Bodega Bay data are being prepared for publication.

1.2 Wind Measurements on a Tall Tower in Rough and Inhomogeneous Terrain

Wind speed and turbulence statistics are often collected at locations marked by both smooth terrain and uniform ground cover for considerable distances upwind from the measurement site. The wind profile and turbulence structure were investigated, based on data from a tall tower.

Averaged wind speed profiles for each sector were constructed from data taken during approximately neutral conditions. Values of the z-intercepts of the various profile segments were assumed to be estimates of the roughness length, z_o.

The average neutral wind speed profiles are shown in figure 3 and the z_o estimates in table 1.

Table 1. Values of z_o for Philadelphia Tower Neutral Wind Profiles

Profile segment (m)	z_o, northerly 1965 data (m)	z_o, northerly 1967 data (m)	z_o, southerly 1965 data (m)	z_o, southerly 1967 data (m)
12.2 - 30.5	___	2.6	___	0.52
12.2 - 61.0	___	2.5	___	___
30.5 - 61.0	2.8	2.2	0.24	0.22
30.5 - 107.0	3.1	2.2	___	___
30.5 - 175.0	3.1	2.5	___	___

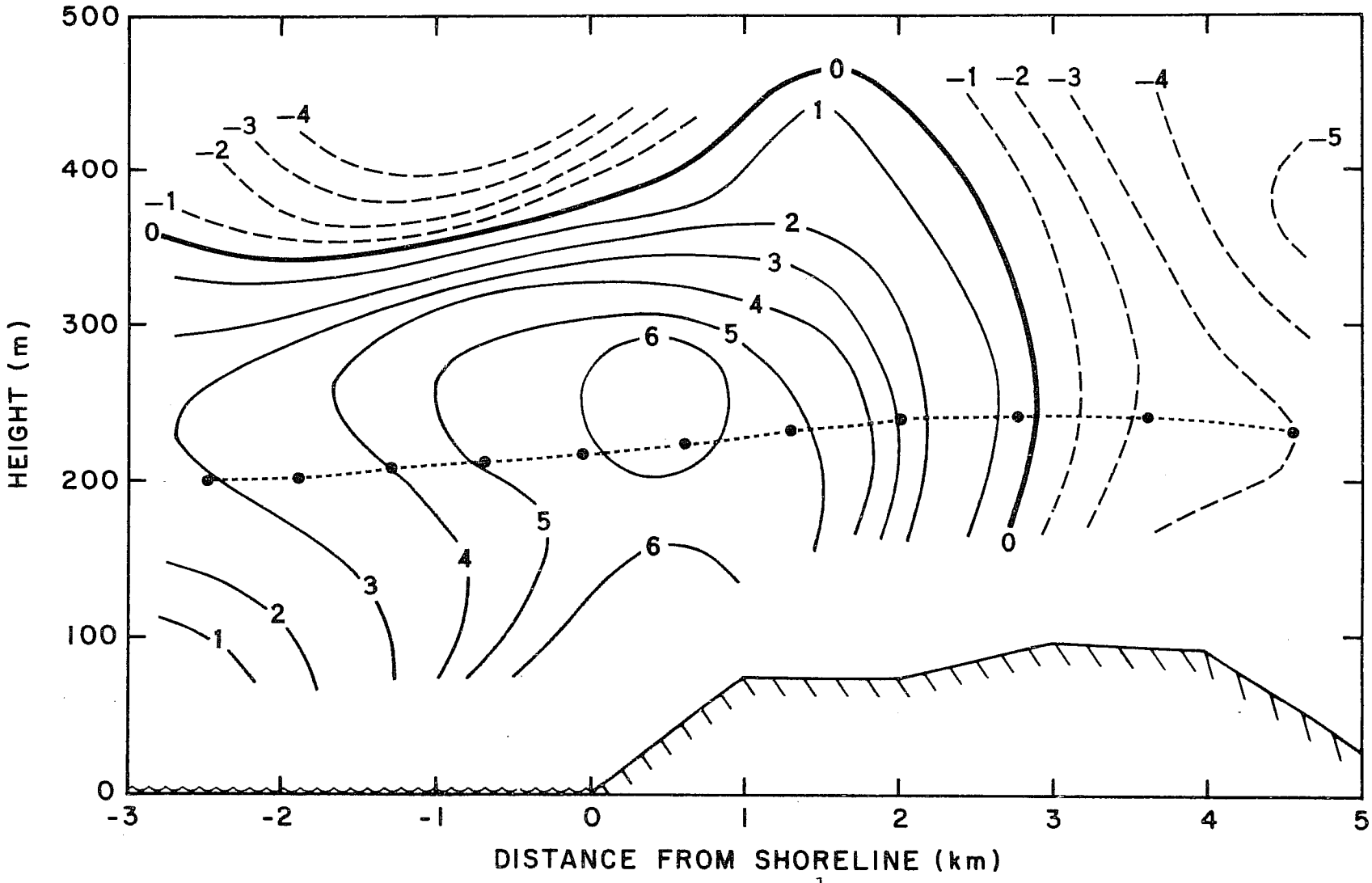

Figure 2. Variation of tetroon-derived vertical velocity (cm s^{-1}) with height and distance from the shoreline at Bodega Bay, California. Positive values signify upward motion. The dotted line, with positions at 2-min intervals, represents the trajectory of an arbitrary air parcel through the mean velocity field. Terrain height indicated by hatching.

The two average northerly profiles appear to be close to logarithmic to about 175 m. The southerly profiles, while similar to each other, display irregularities that may be associated with southerly winds passing over the deep river valley just before arriving at the tower.

The slow-speed (3.0 in./hr) analog wind direction recording was used to estimate σ_θ, the standard deviation of the horizontal wind direction distribution. It was assumed that σ_θ is related to the total wind direction range, R, over some time interval by

$$\sigma_\theta = R/\text{constant}, \tag{2}$$

where a value of 6.0 was used for the constant.

Average estimated values of σ_θ for northerly and southerly flow at the Philadelphia site and data from three very smooth sites are presented in figure 4, which shows that the Philadelphia estimates of σ_θ are considerably larger than the values for the other sites.

Panofsky and Prasad (1965) found that the value of σ_θ can be specified as a function of $\ln z/z_o$ and stability. The σ_θ values in figure 4, all for neutral conditions, were replotted in figure 5 as a function of $\ln z/z_o$. Although the Philadelphia surface conditions differ greatly from those at the other three sites, as evidenced by a range of one or two orders of magnitude in z_o, a considerably better ordering of the rough and smooth site data is achieved.

The wind speed and direction range data obtained at the Philadelphia site may be used to estimate the quantity σ_v/u_*, where u_*, the friction velocity, is obtained from the neutral wind speed profile. If the standard deviation of the lateral velocity, σ_v, is assumed to be given by the product $\sigma_\theta \bar{u}$, where $\bar{u}$ is the mean value of the horizontal wind speed (Lumley and Panofsky, 1964, p. 144), then the values of σ_v and σ_v/u_* for northerly flow at the tower may be calculated. These are given in table 2 and may be compared with those quoted by Lumley and Panofsky (1964, p. 146), which range from 1.3 to 2.6. The Peekskill, New York site, noted by Lumley and Panofsky, is most similar to the Philadelphia location, and the value of $\sigma_v/u_* = 2.0$ found at 91.5 m at Peekskill agrees well with the Philadelphia data.

Of particular interest, in this study, is that concepts usually applied to the atmosphere's surface boundary layer over smooth and regular terrain seem applicable also in a deep layer over quite rough and irregular terrain.

The difficulty of obtaining representative wind profiles in highly irregular terrain may have been resolved by averaging many observations over a broad direction sector, a technique that may find an application in the problem of obtaining representative profiles in urban areas.

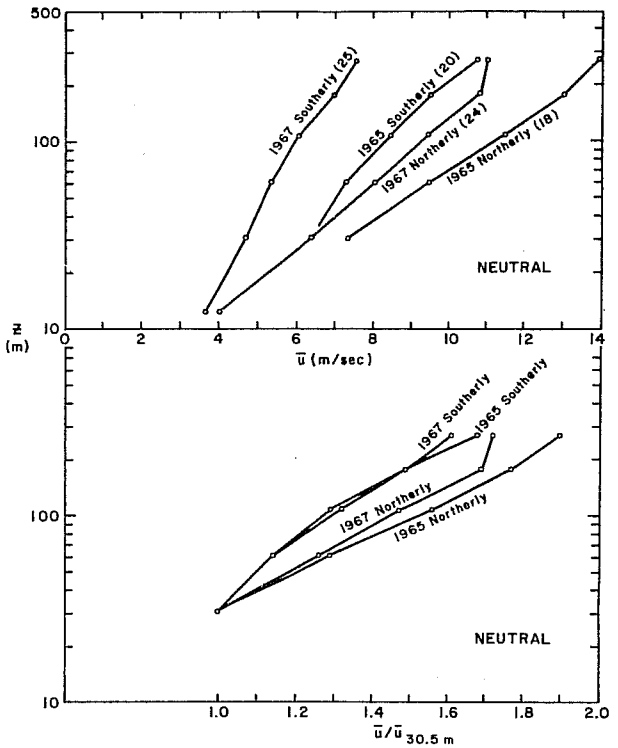

Figure 3. Upper panel: wind profiles observed during neutral conditions at the Philadelphia tower. Lower panel: same profiles divided by speed at 30.5 m. Values in parentheses give total number of hours of data used.

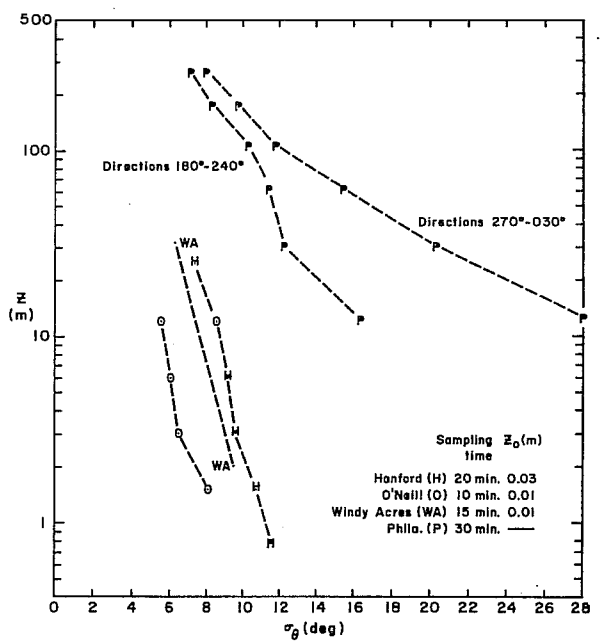

Figure 4. The variation of σ_θ with height during neutral conditions.

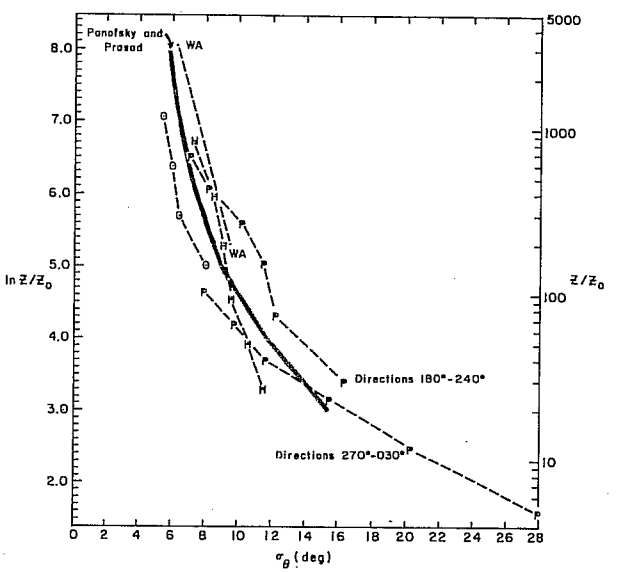

Figure 5. The variation of σ_θ with ln (z/z_o). The data are those plotted in fig. 4.

Table 2. Values of σ_v and σ_v/u_* for Northerly Flow at the Philadelphia Site

height (m)	12.2	30.5	61.0	107	175
σ_v (m/s)	2.00	2.24	2.20	1.94	1.87
σ_v/u_*	1.92	2.15	2.11	1.87	1.80

1.3 Mixing-Length Hypotheses

One series of measurements in 1962 by the Massachusetts Institute of Technology at Round Hill, Massachusetts, has been analyzed. These data consisted of measurements of u, v, w, and T taken every 1.2 s at heights of 16 and 40 m, for approximately 1 hr. The analysis appears to support the modified mixing-length model described previously (ESSA Tech. Memo. ERLTM-ARL 9, 1968). The Kansas data collected by the University of Washington in 1967 are still being analyzed, but a preliminary examination of one run suggests that some of the Round Hill results may be inapplicable because the long (1.2 s) interval between observations does not permit precise determination of derivatives. (The statistics to be examined include correlations between derivatives of different quantities.) The Kansas data, by contrast, have an observation interval of 0.1 s.

1.4 Infrared Hygrometer

Modifications of the ARL infrared Hygrometer were completed in July, and environmental testing began the following month. The principal objectives of the test were to determine the hygrometer's ability to hold dry-point and calibration when subjected to environmental thermal and wind stresses. In order to maintain a constant check, the optical array of the infrared hygrometer was located near the Automatic Meteorological Observation System (AMOS) - 360's dew-cell humidity sensor atop the Gramax Building in Silver Spring, Md. Personnel from the Equipment Development Laboratory of the Weather Bureau operated the AMOS-360. In all, a total of 120 dew-point comparisons were made between August and mid-December, generally between 0900 AM and 0300 PM, EST. Absolute humidity measurements from the infrared hygrometer were converted to dew-point temperature to allow a direct comparison with the AMOS-360 output.

The dew-point temperature comparison (fig. 6) showed a gradual but increasing departure from a one-to-one correlation at lower temperatures. On occasions when the two instruments differed by more than 4°F, a third reading was obtained using a sling psychrometer. This value generally agreed with the infrared hygrometer reading. The excessive dew-point temperature values from the AMOS-360 are believed to be caused by a "hysteresis" in the

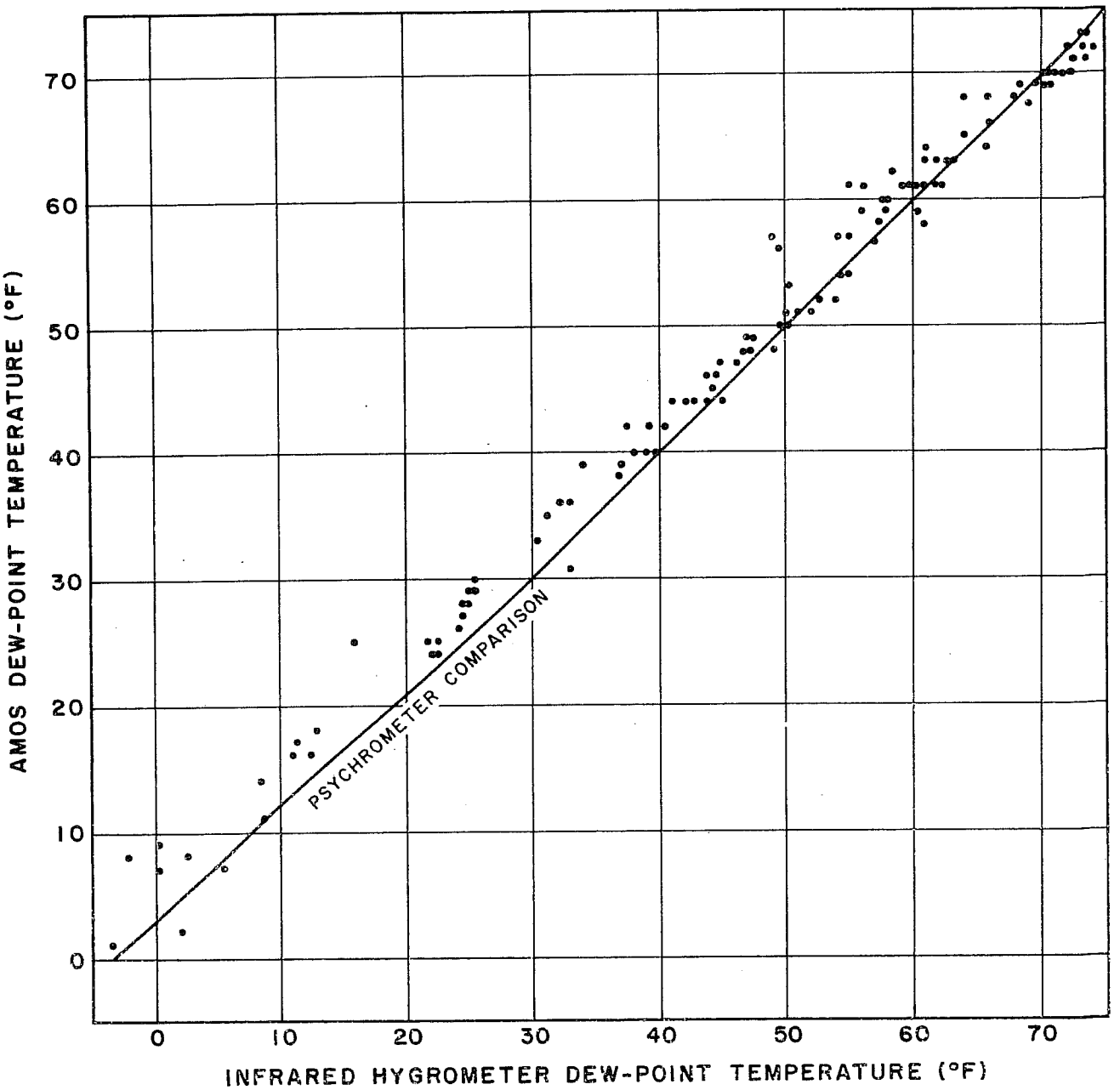

Figure 6. Dew-point temperature comparison as measured by infrared hygrometer and dew-cell humidity sensor.

heating-cooling cycle of the dew-cell hygrometer. For comparative purposes, the results of an earlier study, using a sling psychometer as a reference, were also presented in figure 6 (solid line). In this test, conducted in the spring of 1966 in an open field near Dulles Airport, a one-to-one correlation was observed down to about 30^{o}F.

In all respects, the infrared hygrometer performed well throughout the entire test period. The dry-point reading remained unchanged, and the calibration was varified from 5 g m^{-3} to 25 g m^{-3} of water vapor. At the conclusion of these tests the instrument was sent to the Idaho office for use in conjunction with deposition studies.

2.0 RESEARCH AT NATIONAL REACTOR TESTING STATION, IDAHO

2.1 Diffusion and Deposition Comparison Studies

A check on the validity of using a uranine dye derived deposition and diffusion climatology for estimating deposition and diffusion of molecular iodine has been attempted. For study of interaction between uranine dye and molecular iodine, paired tracers — uranine dye and methyl iodide, and molecular iodine and methyl iodide — have been released in the atmosphere. (Methyl iodide is a nondepositing tracer.) The results of these field releases are summarized below.

Except under most steady conditions, e.g., constant components of turbulence intensity throughout sub-intervals of the diffusing period, relative differences in tracer release rates can profoundly affect the sampled effluents and the diffusion and deposition comparisons based on these sampled effluents. This lack of steadiness seriously affected the sampled concentrations from the molecular iodine and methyl iodide paired tracer experiment, called CDT III. Time variations in the tracer release rates were accompanied by significant time variations in wind direction and speed. Consequently, molecular iodone was released under substantially different conditions than methyl iodide, and a meaningful comparison cannot be made between the two tracers. Better controlled release techniques have been developed and will be used in a repeat methyl iodide-molecular iodine experiment in the spring of 1969.

Lateral diffusion results of the methyl iodide-uranine dye experiment (CDT II)are compared in table 3. The lateral diffusion parameter, σ_y, for uranine dye is comparable to, but smaller than, the values calculated for methyl iodide. The ratio of σ_y dye to σ_y methyl iodide is also shown. At 1600 m downwind a substantial difference exists, probably as a result of the depletion of the uranine dye plume. Table 3 also lists effective values of σ_z, the vertical diffusion index, for methyl iodide, calculated from the crosswind integrated concentration (CIC).

Table 3. Lateral Diffusion, σ_y, and Vertical Diffusion, σ_z

	Lateral Diffusion (m)			Vertical Diffusion (m)
			Dye/CH_3I	
Distance (m)	CH_3I	Dye	Ratio	CH_3I
100	29	24	.83	7
200	45	43	.96	15
400	78	75	.96	57
800	177	163	.92	146
1600	396	258	.65	356
3200	884	-	-	467

Table 4. Comparison of CIC $\bar{U}/Q$ Values

	Distance (m)					
Tracer	50	100	200	400	800	1600
CH_3I*	146	117	54.5	14.0	5.5	2.3
Dye*	52.6	33.8	11.9	3.1	1.2	0.5
Ratio CH_3I/Dye	2.8	3.4	4.6	4.5	4.6	4.6
Cumulative Fract. Depletion	.64	.71	.78	.78	.78	.78

*Based on samples collected at 1-m heights. units are m x 10^{-3}.

Table 4 compares normalized CIC for the effluents collected at 1-m heights on the concentric sampling arcs. At 200 m and further downwind, about 4.5 times more methyl iodide than uranine dye seems to be present.

Samples collected on the four 100-ft towers 385 m downwind are summarized in table 5. A summation of all uranine dye collected by tower samplers is proportional to the amount of tracer remaining airborne at that distance. When the sum of all tower-sampled methyl iodide is divided by the sum of all tower-collected uranine dye, the ratio agrees almost exactly with the CIC ratio shown in table 4 for the 400-m arc. This agreement suggests that the difference between vertical diffusion of uranine dye and methyl iodide is the result of deposition of the uranine dye within the first 200 m of travel. The mass median diameter of the uranine dye is 1μ with a gravitational settling velocity of 15 cm/hr. Thus, for the CDT II experiment the dye would fall 0.2 cm in the time required to reach the 200-m arc. Therefore, the gravitational effect could not be expected to contribute significantly to the deposition factor. The cumulative fractional depletion of the uranine dye plume is represented by 1 minus the ratio of dye CIC to methyl CIC. The last line of table 4 lists the depletion factors. For this case, more than half the dye is deposited with the first 50 m of travel. Beyond 800 m downwind the analysis of the data shows a noticeable lack of dye depletion. It is not yet clear what combination of effects causes this phenomenon.

The uranine dye deposition velocity calculated at 100 m downwind was 8 cm/sec, which is comparable to some values calculated by Islitzer and Dumbauld (1963) for uranine dye releases under unstable temperature lapse conditions. Deposition velocities at 50 m downwind were estimated to be three to five times greater than the 100-m value. The repeat dual release of methyl iodide and molecular iodine will be examined for this effect, based on carbon fallout plates, grass, and soil samples close to the source.

2.2 Mesoscale Wind Field, Transport, and Diffusion Studies

Use of wind direction and velocity data, reported from 19 wind stations positioned over the Snake River Plain of southeastern Idaho has been proposed for study of mesoscale wind circulations as well as transport and dispersion (ESSA Tech. Memo. ERLTM-ARL 9, 1968). The winds at individual points on a rectangular grid were obtained by a technique involving weighted averages of wind data from the irregularly spaced stations within a specified distance of each grid point. The weighting factor was the reciprocal of the station distance raised to some specified power. Time series of the interpolated wind data on the grid points were also used to construct trajectories of hypothetical particles, and computer programs were developed to automatically display the wind fields and trajectories.

A major concern is the validity of the interpolation of randomly spaced data to a rectangular grid. Tests were conducted in which exponents of 1, 2, and 3 were used on the reciprocal of the distance. The second power was found to provide the most satisfactory results, in agreement with the findings by Shepard (1968). One other technique was tested for feasibility, which

Table 5. Tower Values of $\chi\bar{u}/Q$*

	Sfc.		20'		40'		60'		80'		100'	
Tower	M	D	M	D	M	D	M	D	M	D	M	D
1	2.9	.68	3.2	.52	2.1	.68	1.6	.52	3.5	.39	2.0	.51
2	4.9	.93	2.7	.85	3.9	1.1	3.9	1.0	4.1	1.1	3.2	.79
3	8.2	2.0	8.2	2.0	10.3	1.8	8.6	1.4	6.1	1.6	6.1	1.4
4	9.4	1.8	M	M	10.2	1.7	8.0	1.4	M	M	6.9	1.7
Sum	25.4	5.41	14.1	3.37	26.5	5.28	22.1	4.32	13.7	3.09	18.2	4.40

Sum of all methyl = 120.0

Sum of all dye = 25.87

Ratio (all methyl/dye) = 4.63

* All $\chi\bar{u}/Q$ values x 10^{-5} with units $(m)^{-2}$

involved connecting pairs of data points until the section of the plane containing the points had been partitioned into triangles. The interpolated data value at a grid point falling within the boundaries of a triangle was obtained by assuming that it was on the plane defined by the data values at the verticies of the triangle. Examples of the two types of interpolation are shown in figures 7 and 8. The patterns are quite similar, except for a slightly sharper region of shear for the triangle method, as seen in the center portion of figure 8. The logic required to program the method of triangles increased the computer time by a factor of four, however, and the problem of sporadically missing data would require a fairly frequent redefinition of the triangular areas. Thus the weighted average technique was selected for future use. Improvements in this technique are being tested for possible incorporation into the program.

The hourly averaged data extracted from the strip charts of each station are edited and put on magnetic tape in a form readily available for computing the wind fields. An hourly inventory of the data is printed out as the punched cards are batched onto tape; it is compact enough to allow 8 days of record per page, and thus the patterns of the missing data become evident.

The data from the network of stations are being used in a feasibility study of mesoscale flow characteristics, such as divergence and vorticity. Since these quantities are influenced somewhat by the objective analysis of the wind data, a comparison with values computed independently from tetroon data should indicate the validity of the analysis. The divergence values may be used for rough estimates of average mesoscale vertical velocity. The relationship used is

$$W_D = W_O - \left(\frac{\partial u}{\partial x} + \frac{\partial V}{\partial y}\right) \cdot D, \qquad (3)$$

where W_D is the vertical velocity at the top of a layer of thickness D, W_O is the vertical velocity at the ground due to the slope of the surface and the speed of the wind, and $\left(\frac{\partial u}{\partial x} + \frac{\partial v}{\partial y}\right)$ represents the mean value of the horizontal component of divergence in the layer.

Values of divergence and vorticity were computed for 12 consecutive hourly averaged wind fields. The patterns for both quantities were reasonably consistent from one field to the next, except for one case in which a frontal passage at the upper end of the valley was represented by only one station. The situation has been somewhat improved by the addition of three additional stations in this portion of the grid. The magnitude of the divergence values was checked by assuming the layer thickness D to be 200 ft and examing the resulting magnitudes of $W_D - W_O$. The vertical velocity difference, $W_D - W_O$, had extreme values from -4 to + 10 cm/sec over the 12 cases. The vertical velocity at ground level, W_O, which will depend on the speed and direction of the wind and slope of the ground, is estimated to have a range on the order of -8 to +8 cm/sec. The topography is being entered into the analysis to be considered with the divergence calculations. The effects of convection have not yet been considered.

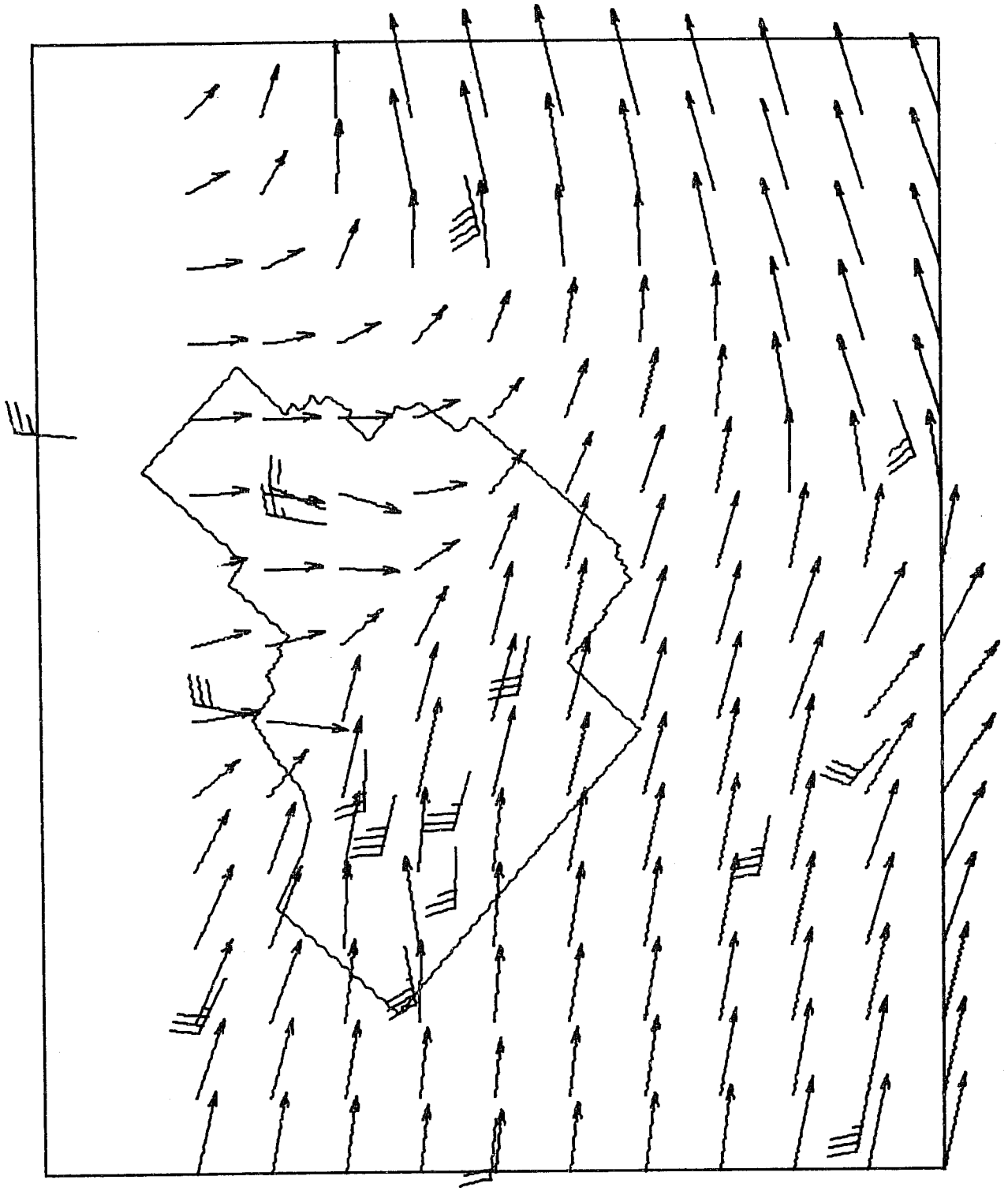

Figure 7. Mesoscale flow pattern depicted by wind vectors obtained by objective interpolation of 10-min average winds. The standard wind symbols represent the raw data and the vectors represent the interpolated data.

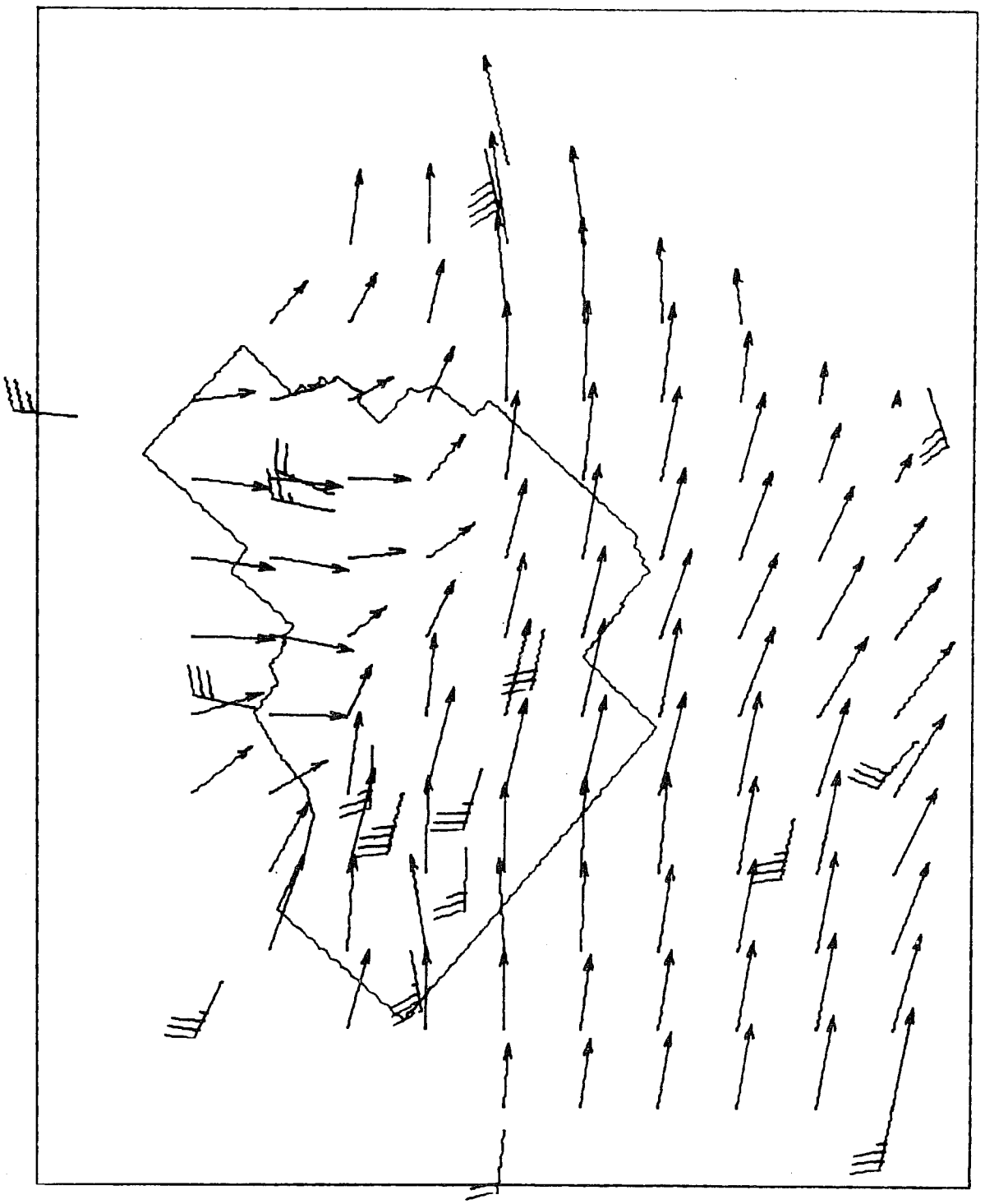

Figure 8. Same as fig. 7, except that the grid point winds from the wind station data were obtained by the triangular method of interpolation.

The graphical presentation of the trajectories of hypothetical particles, constructed from sequential wind fields, has been modified. An example is shown in figure 9. This series of trajectories indicates the paths followed by 11 particles released serially 1 hour apart from a reactor area at the southwest portion of the NRTS. The numbers at the ends of the trajectories indicate the order of release. The corresponding times are shown in the lower right corner of the diagram. The letters along the trajectories indicate particle position corresponding to the times indicated in the table. By connecting like letters on different trajectories, a time sequence of approximate plume center lines may be visualized. The diagram may also be used to show the advantage of using a wind field analysis, instead of the winds at a single station, to construct trajectories 6, 7, and 8 with the same sequences on trajectories 9, 10, and 11.

A sequence like the one shown in figure 9 gives a general indication of the area over which material might be carried and dispersed by the flow field. There is no indication, however, of the dilution of the concentration of the material by turbulent motion of a scale too small to be represented by sparsely scattered wind stations. For a first estimate of the dosage patterns produced by a released effluent, the advection process reflected by trajectory construction from the wind fields has therefore been incorporated into a diffusion model (Dickson, 1967).

The digital computer model used for the diffusion calculations handles all plumes as a finite number of instantaneous puffs released over an appropriate time interval. In this way, the dilution of the effluent is calculated for a plume dispersed by a wind field that varies in both time and space. The total integrated effluent concentration is approximated by the time-weighted summation of the shorter time effects of each individual puff.

The diffusion model also accounts for hourly changes in a Pasquill type diffusion class, the vertical depths of the mechanically and convectively mixed atmospheric boundary layer, and the release height, strength, duration of the source. The size and density of a rectangular array of surrounding receptor points are selectable initial conditions.

The total-integrated relative concentration has been calculated for the flow patterns illustrated in figure 10. In the subsequent illustrations a unit rate of release has been assumed for the entire 11-hour period, which is analogous to a plant operation restricted primarily to lapse conditions.

As the effluent is transported and diffused through the computational area shown in figure 11, the summed effect is retained at each receptor point. At desired intervals of transport time the accumulated effluent exposure for each point is listed by the computer.

Figure 12 illustrates the contoured format of the output exposure information for 1330 local time, or 4 hours after the beginning of effluent release. Each receptor point is printed and identified by the numbered coordinates along the top and left edges. Each contour of time accumulated

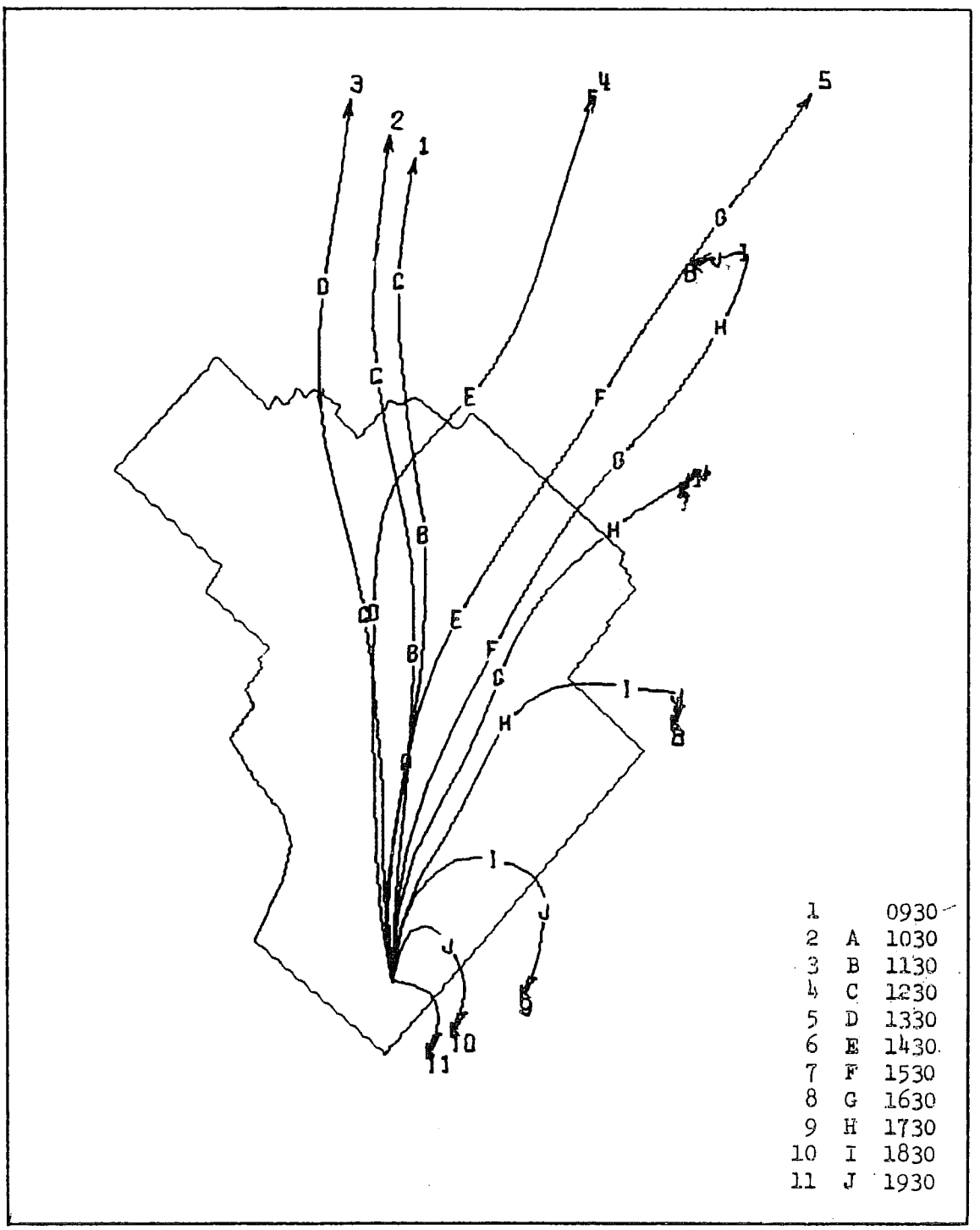

Figure 9. Trajectories of hypothetical particles released into a time series of objectively interpolated wind fields.

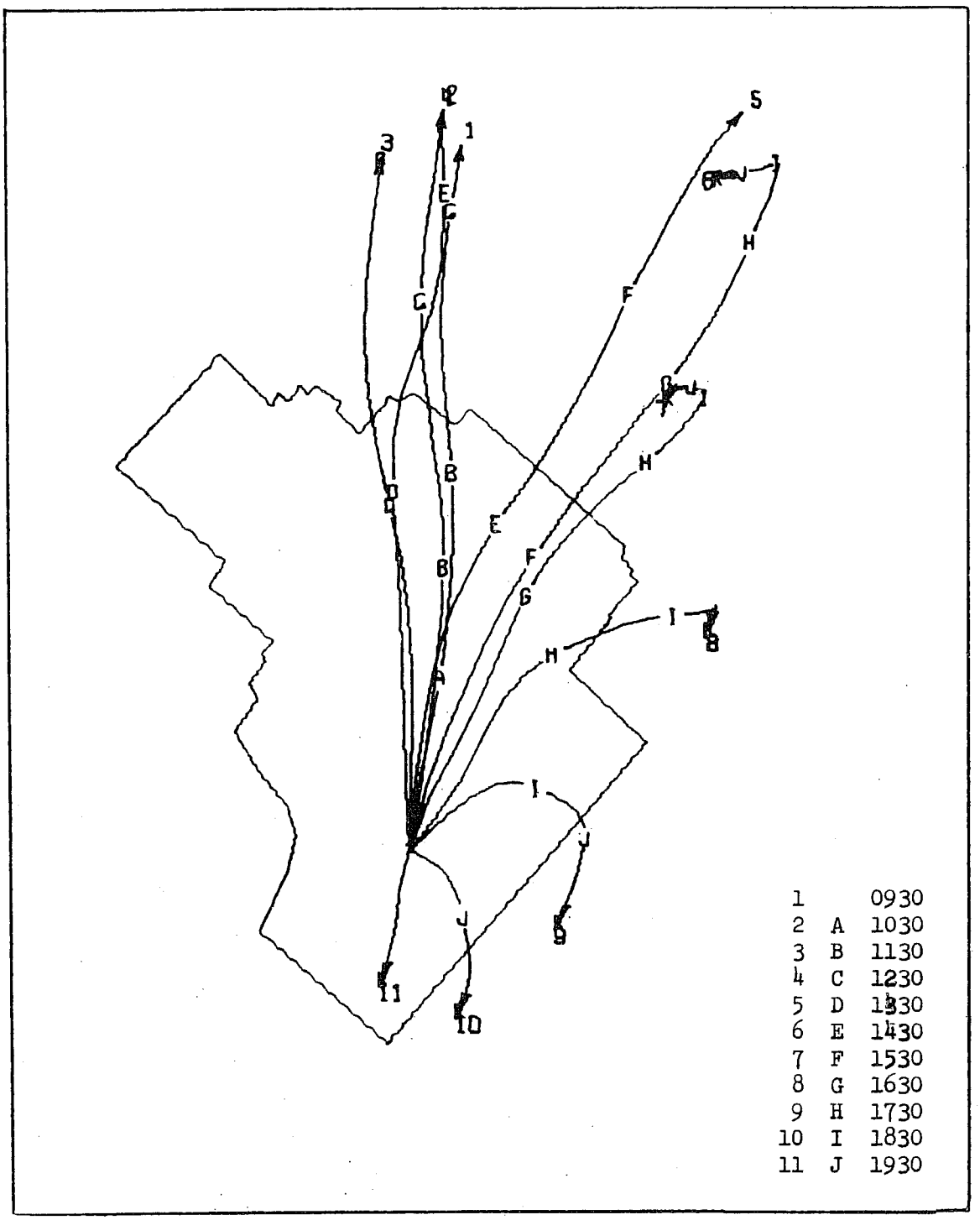

Figure 10. Trajectories of hypothetical particles with ISPP assumed as the source.

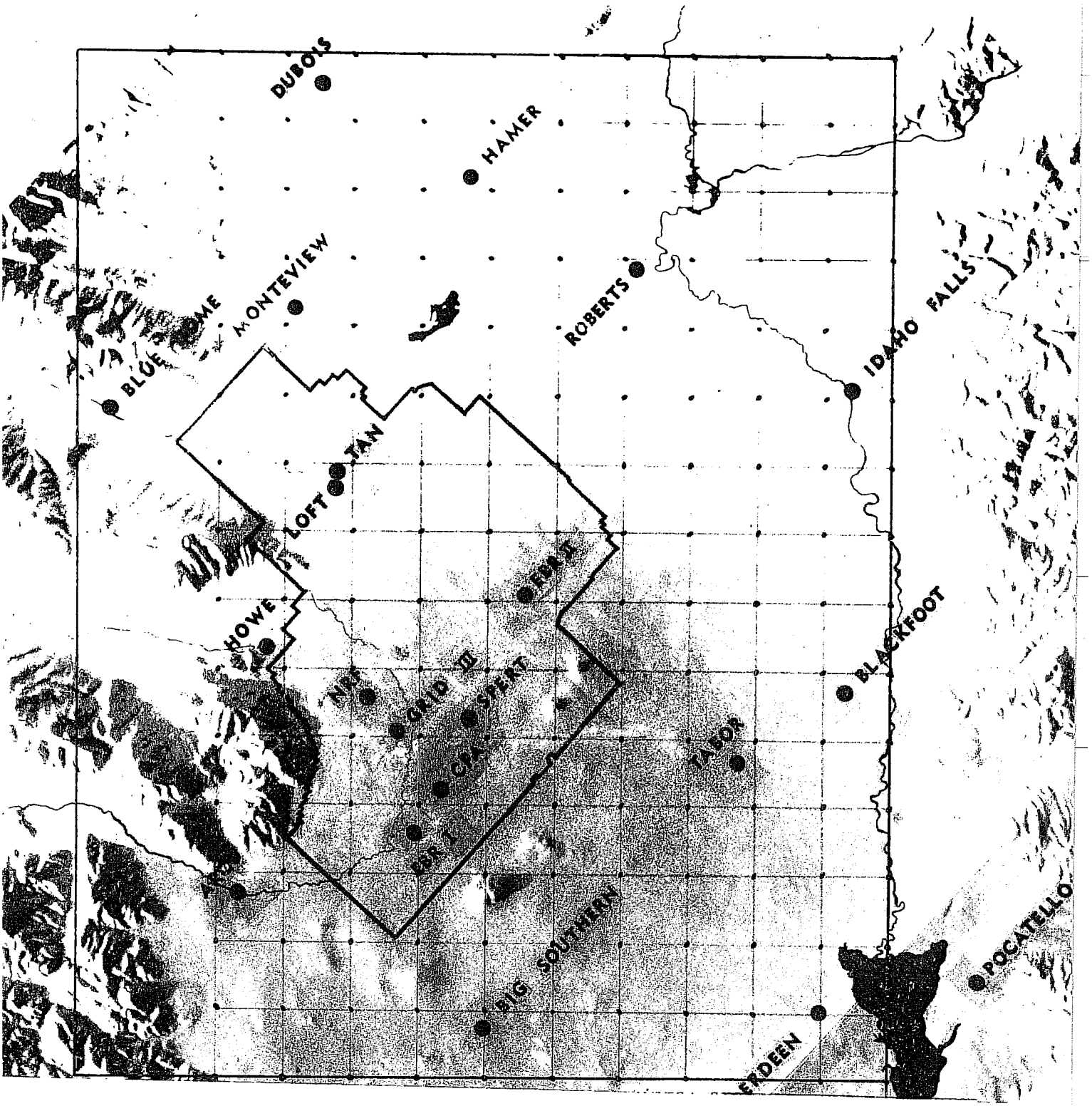

Figure 11. The geographical extent of the computational area.

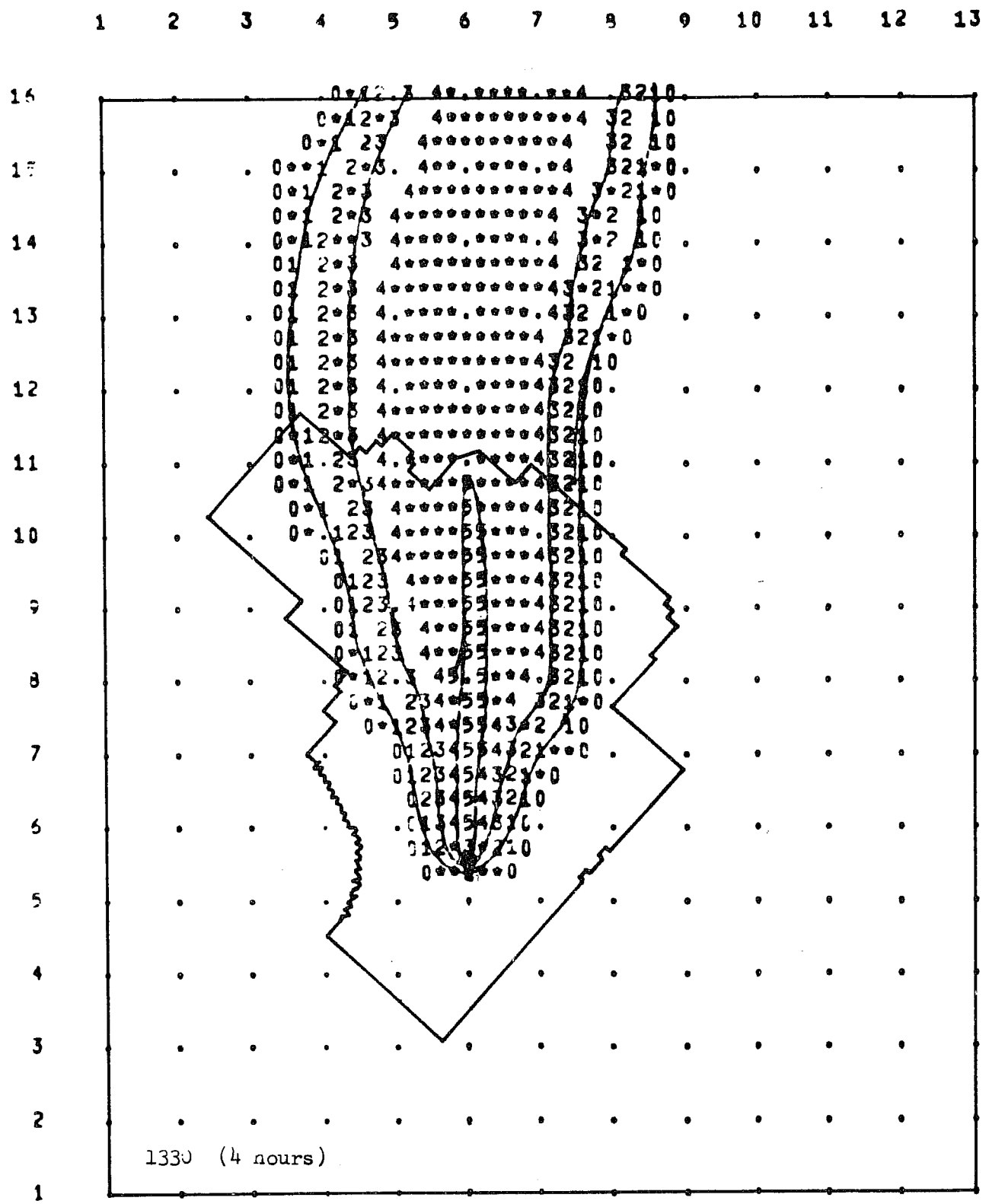

Figure 12. Contoured output format of effluent exposure pattern 4 hours after the beginning of the hypothetical release.

effluent exposure is denoted by the patterns of a particular integer. In this illustration, the integer zero represents accumulated relative concentrations of 1×10^{-18} (hr/m^3). For larger integers the contour values are larger. Alternate intervals between contours have been shaded by star symbols for greater resolution. The zone of greatest exposure (integer 5) lies northeast of the source along the prevailing wind, as expected.

Figure 13 shows the exposure pattern at 1730 local time, or 8 hours after the beginning of the effluent release. The zone of greatest exposure is now a forked pattern because of a rather rapid shift of wind direction from southwesterly to nearly westerly.

In figure 14 the winds within the computation mesh have become northeasterly or very light. After 11 hours of effluent release (2030 local time) this exposure pattern has developed. At nightfall the rate of atmospheric diffusion has slowed and relatively high exposure levels have been accumulated south of the source — position (6, 5.5) on the mesh. During the last 3 hours virtually no additional effluent has been transported into the region east-northeast of the source. Referring back to figures 11 and 13 (3 hours earlier), note the position of the "5" contour line over EBR-II and off-site toward Roberts. Then note in figure 14 the sizable growth of this contour. A considerable amount of this growth to the east of the site has resulted from the plume remaining nearly stationary over this area. The use of a wind observed at the source and applied to the entire area would not have given the same results.

This detailed information is available only by use of electronic computers, which can perform such computations within 5 min or less.

During the next phase of this project, real effluent release rates will be used for the model source and the calculated time accumulated effluent exposures will be compared with a number of air quality measurements for points within the same computational area.

2.3 Feasibility of an Automatic Tetroon Release System

An automatic tetroon release upon receipt of an alarm signal is being considered. The hope is that under stable conditions the tetroon can fly relatively close to the ground, say less than 200 m, and thereby serve as a tracer for plume transport. Under unstable conditions, the mean flight altitude of the balloon should be within the mixed layer to serve as a tracer of a plume.

There are two primary problems. The first, which is only to be mentioned, is that a tetroon is likely to be brought to the earth's surface in thermal convection regimes, particulary if the density level at which it is supposed to fly is near the surface. If the tetroon is being skin tracked and is not burst by sticks or stones, the test may resume as soon as the balloon gains sufficient altitude. If tracked by a transponder, the tetroon's collison with the ground would probably end the test. The second problem, to be considered in some detail, is whether the equilibrium flight altitude of preinflated

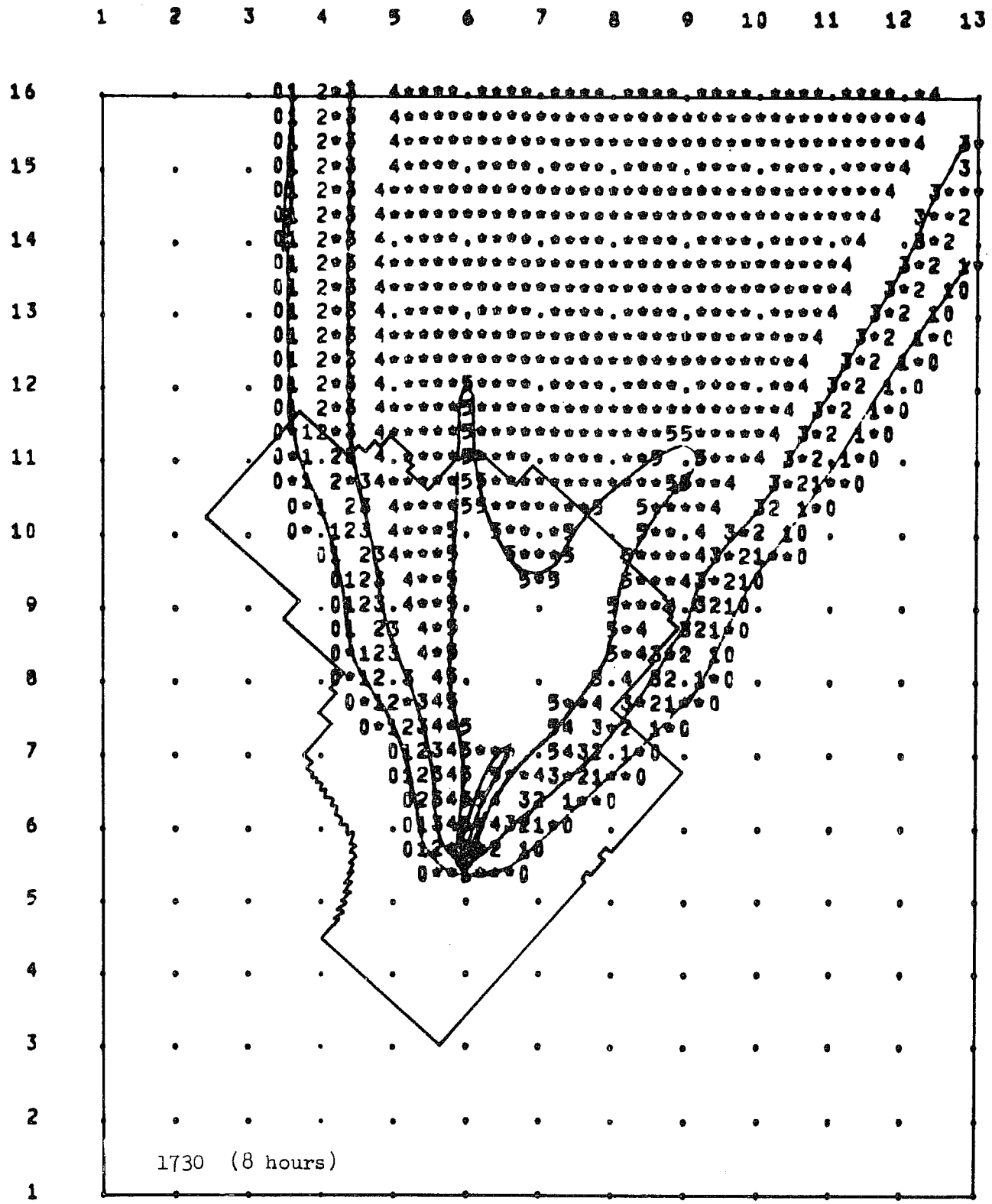

Figure 13. Same as fig. 12, except for 8 hours after the beginning of the release.

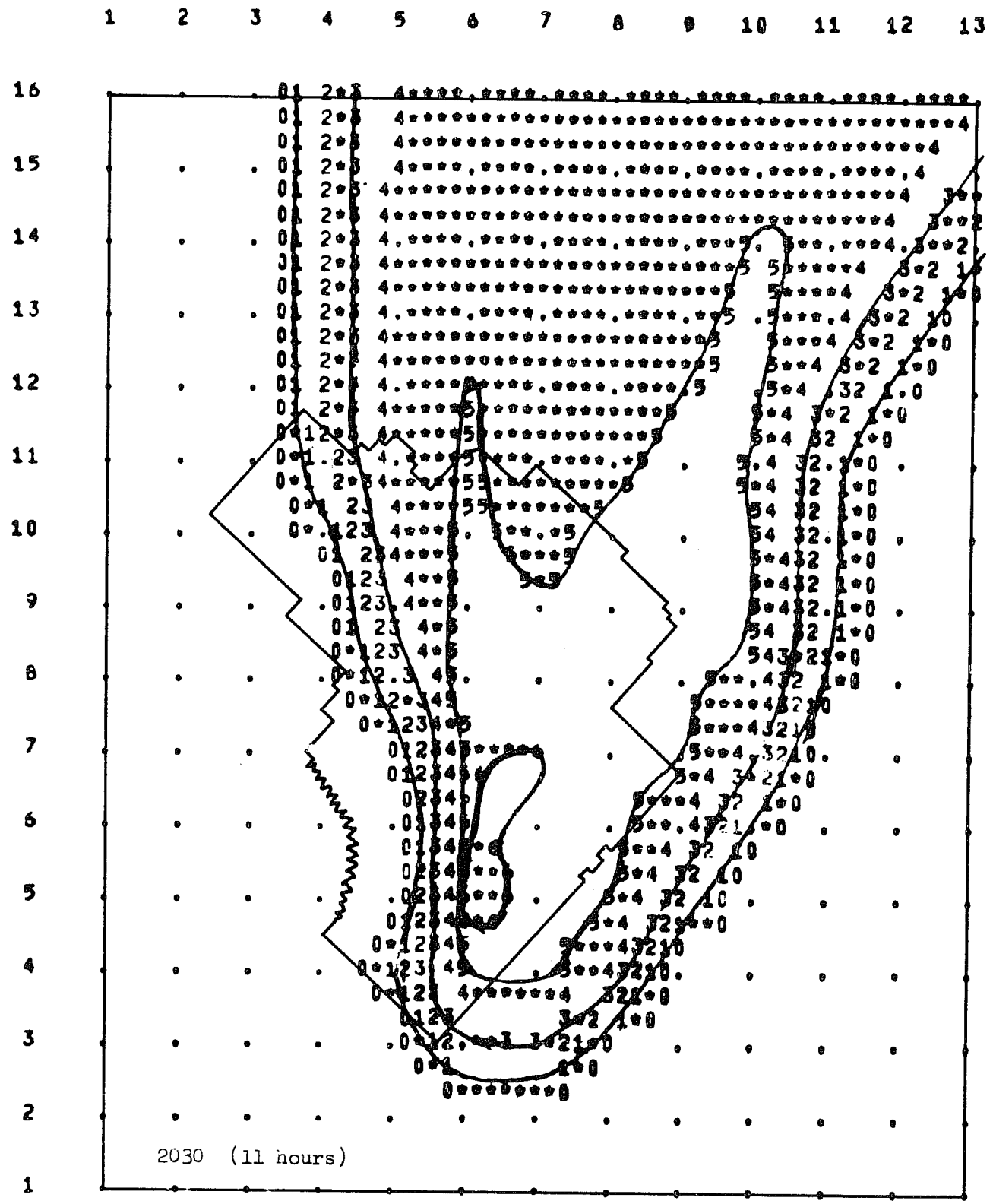

Figure 14. Same as fig. 12, except for 11 hours after the beginning of the release.

tetroons is sufficiently steady to allow the tetroons to fly at altitudes where the trajectory will realistically simulate the plume transport.

The equation of buoyancy is

$$L_n = L_g - B$$

or (4)

$$L_n = V(\rho_a - \rho_g) - B,$$

where L_n is the net lift of the tetroon and its train, L_g is the gross lift, B is the combined weights of balloon, ballast, and instrument, V is the tetroon volume, ρ_a is the ambient air density, and ρ_g is the inflation gas density. The assumption is that the balloon may be safely filled to sufficient superpressure to remain unattended for considerable periods and never encounter temperatures that would allow the volume to slacken. Differentiating (4) with respect to altitude (Z) we get

$$\frac{\partial L_n}{\partial Z} = (\rho_a - \rho_g) \frac{\partial V}{\partial Z} + V \frac{\partial}{\partial Z} (\rho_a - \rho_g), \tag{5}$$

and assuming $\frac{\partial V}{\partial Z}$ and $\frac{\partial \rho_g}{\partial Z}$ to be negligible in the 500 m above the ground, we have

$$\frac{\partial L_n}{\partial Z} = V \frac{\partial \rho_a}{\partial Z} . \tag{6}$$

Assuming the rate of change of L_n with altitude is linear through the layer gives

$$\Delta Z = \frac{L_{ni}}{V} \left(\frac{\partial \rho_a}{\partial Z} \right)^{-1} , \tag{7}$$

where L_{ni} is the initial free lift, and ΔZ becomes the equilibrium flight altitude where $L_n = 0$.

If tetroons are preinflated and left unattended until released by some alarm, they may be considered preset to fly at a given density level. Three years (1961-1963) of Boise radiosonde observations were analyzed to determine averages, variances, and extremes in the heights of a density surface. Table 6 shows the height analysis for the 1.0×10^{-3} density surface, figures 15 to 18 show the individual observations for 4 months in 1961, and figure 19 shows the individual observations for the entire year 1961, revealing clearly the seasonal trends. Solid lines are 0000Z observations; dots are 1200Z observations. The extremes in table 6 are 1064 m (ASL) on the afternoon

Table 4. Analysis of the Height, in Meters Above Sea Level, of the 1.0×10^{-3} Density Surface Over Boise, Idaho.

		0000Z				1200Z			
Year	Month	Mean	Std. Dev.	Max.	Min.	Mean	Std. Dev.	Max.	Min.
1961	1	2205	131	2507	1988	2217	130	2491	1952
	2	2212	143	2416	1841	2240	154	2457	1787
	3	2138	165	2389	1746	2162	154	2421	1751
	4	2029	145	2261	1675	2102	173	2375	1752
	5	1814	234	2232	1309	1937	191	2263	1551
	6	1414	211	1827	1088	1575	157	1942	1413
	7	1385	155	1839	1088	1513	101	1772	1326
	8	1373	132	1647	1064	1518	99	1712	1300
	9	1794	198	2189	1423	1877	198	2255	1524
	10	1967	220	2352	1528	1999	201	2367	1636
	11	2138	175	2425	1868	2185	173	2441	1852
	12	2296	175	2606	2005	2319	163	2731	2064
1962	1	2332	162	2708	2077	2349	179	2709	2010
	2	2182	199	2666	1907	2222	193	2726	1967
	3	2209	141	2516	1907	2242	149	2525	1939
	4	1914	235	2280	1407	1999	192	2341	1612
	5	1859	147	2145	1525	1948	89	2131	1817
	6	1622	223	2064	1126	1735	196	2177	1411
	7	1500	151	1789	1226	1629	139	1954	1408
	8	1529	190	1870	1223	1666	156	1970	1374
	9	1613	157	2139	1399	1705	156	2130	1511
	10	1867	170	2262	1371	1920	107	2242	1722
	11	2104	185	2427	1812	2118	170	2407	1834
	12	2165	157	2472	1865	2194	149	2525	1939
1963	1	2334	192	2838	2075	2338	189	2847	2007
	2	2114	161	2356	1729	2139	150	2397	1840
	3	2132	171	2385	1756	2184	148	2434	1814
	4	2089	179	2359	1633	2117	184	2363	1637
	5	1797	180	2137	1505	1869	150	2163	1652
	6	1725	187	2036	1390	1808	159	2021	1510
	7	1511	167	1837	1164	1625	123	1875	1416
	8	1441	164	1782	1140	1598	111	1812	1448
	9	1574	199	1926	1200	1677	167	1936	1402
	10	1803	237	2239	1326	1869	196	2273	1525
	11	2090	162	2386	1681	2102	152	2392	1777
	12	2226	121	2518	1974	2223	116	2554	2026

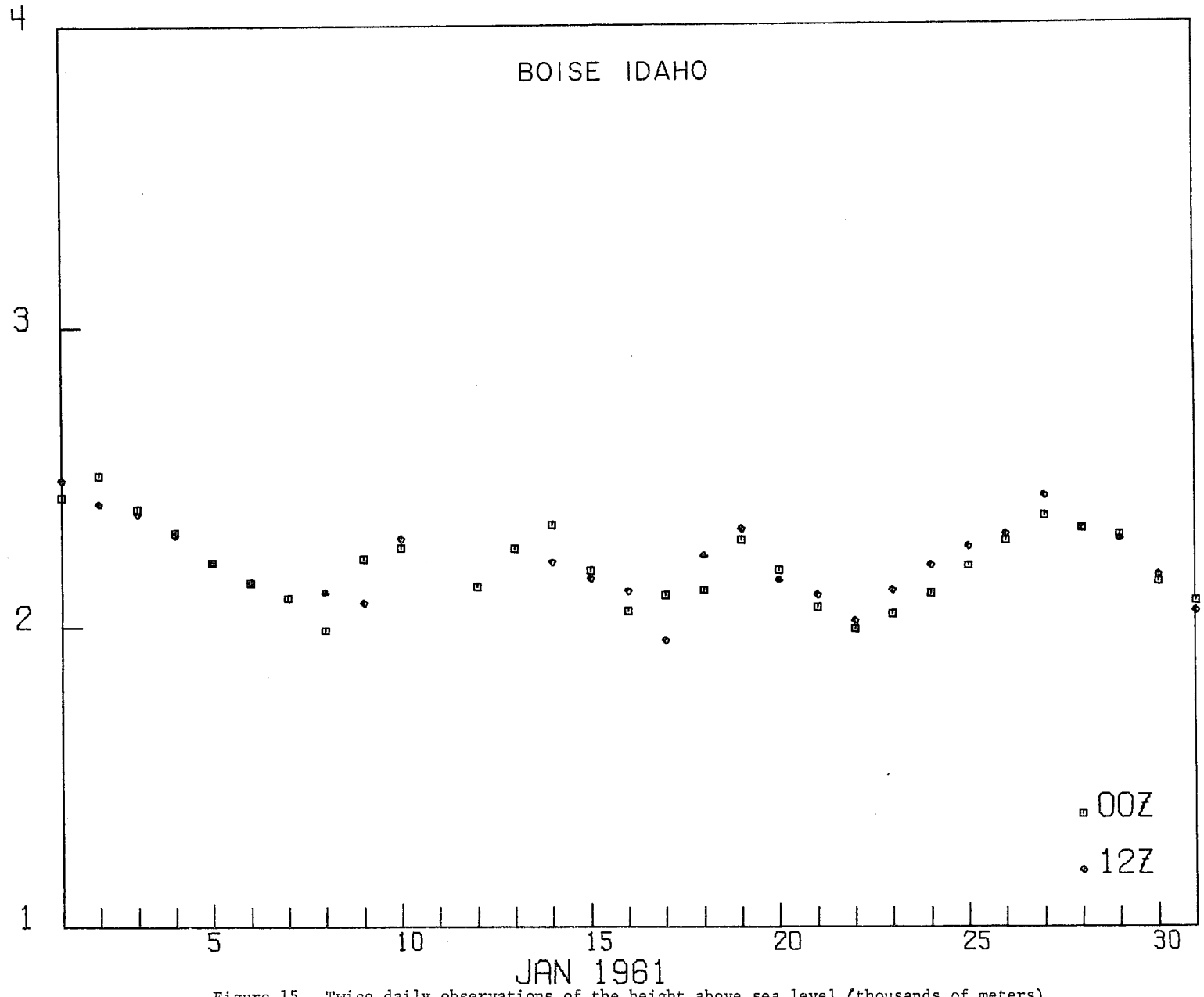

Figure 15. Twice daily observations of the height above sea level (thousands of meters) of the 1.0 x 10^{-3} g/cm^{-3} density level at Boise, Idaho, January 1961.

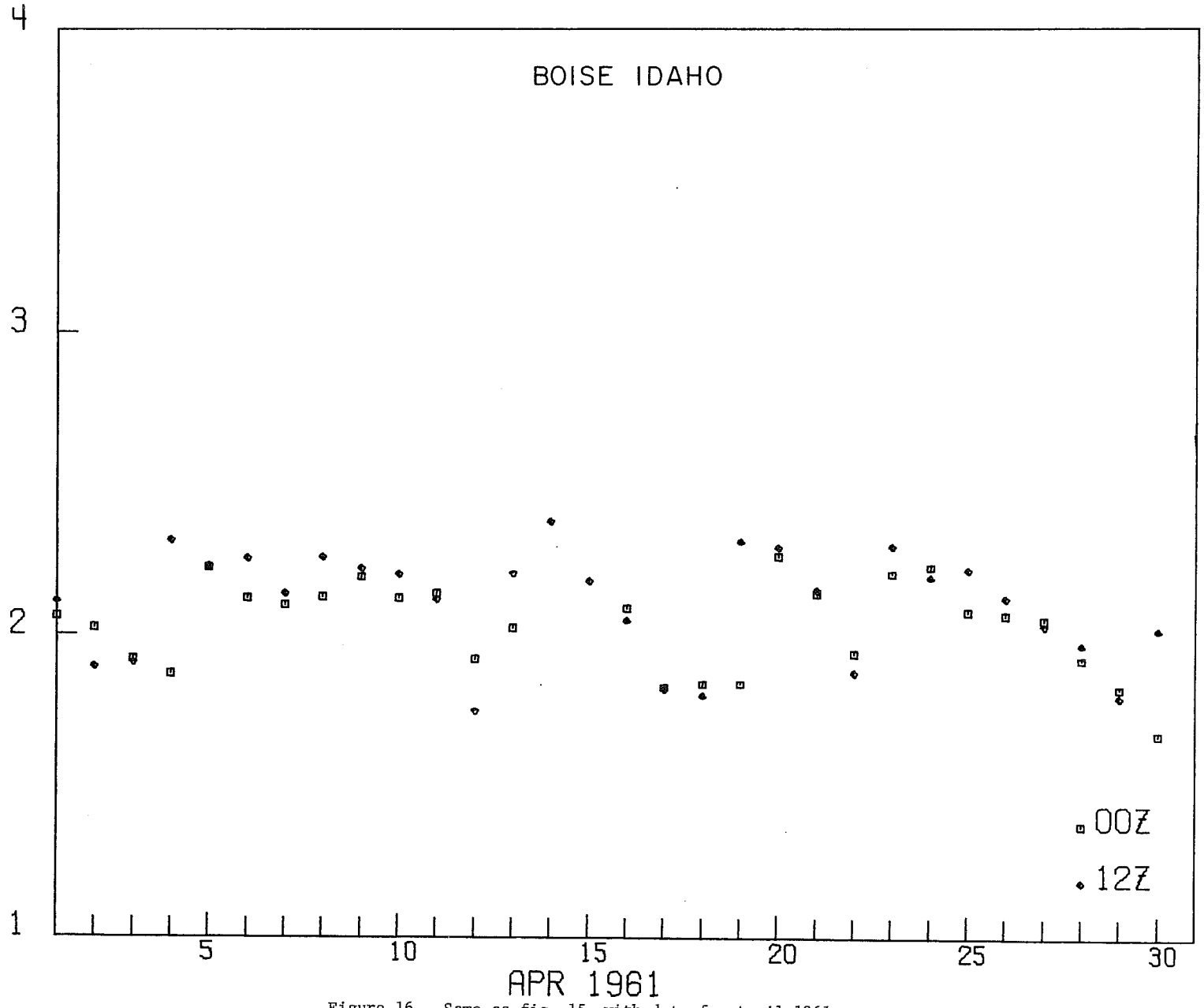

Figure 16. Same as fig. 15, with data for April 1961.

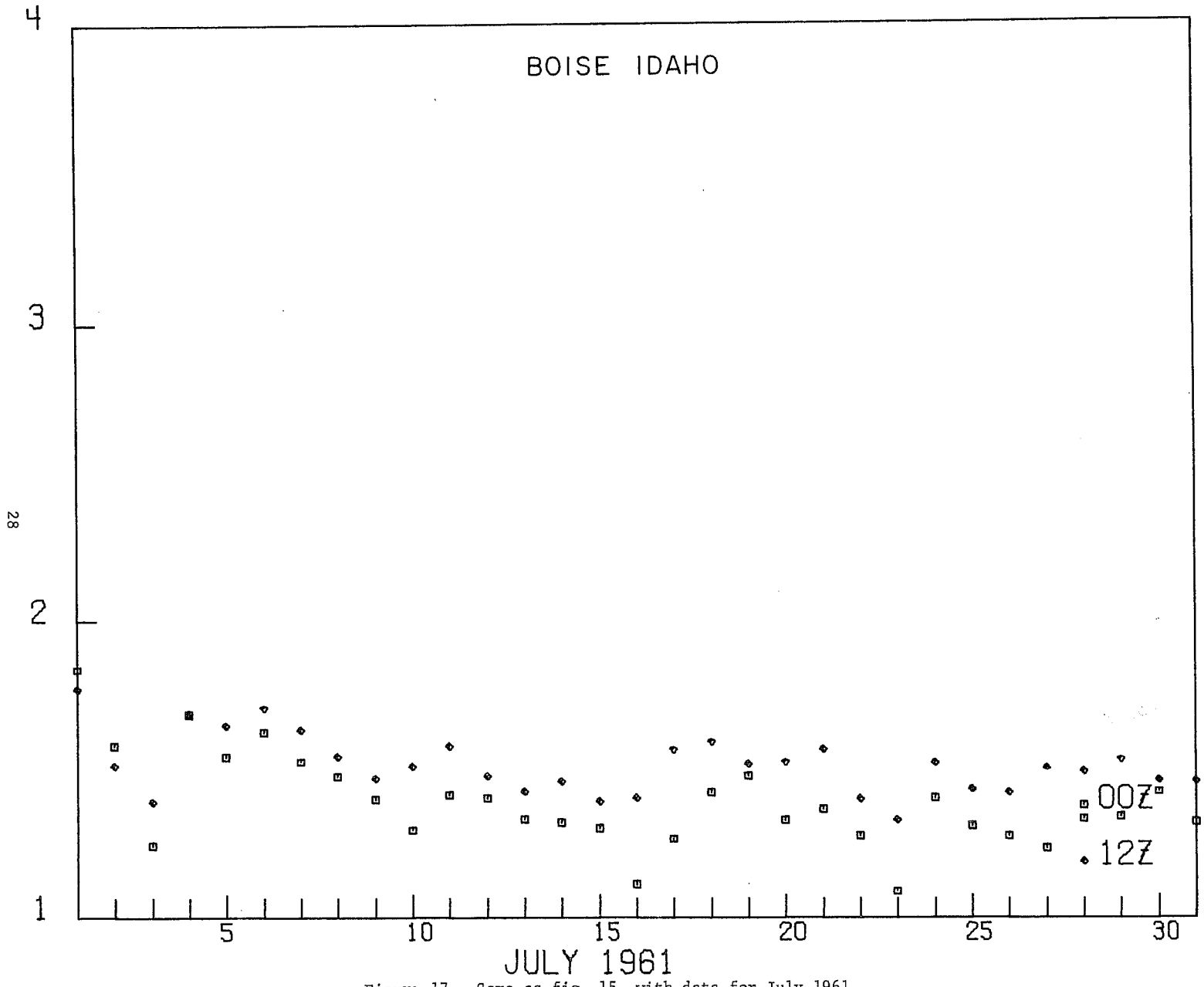

Figure 17. Same as fig. 15, with data for July 1961.

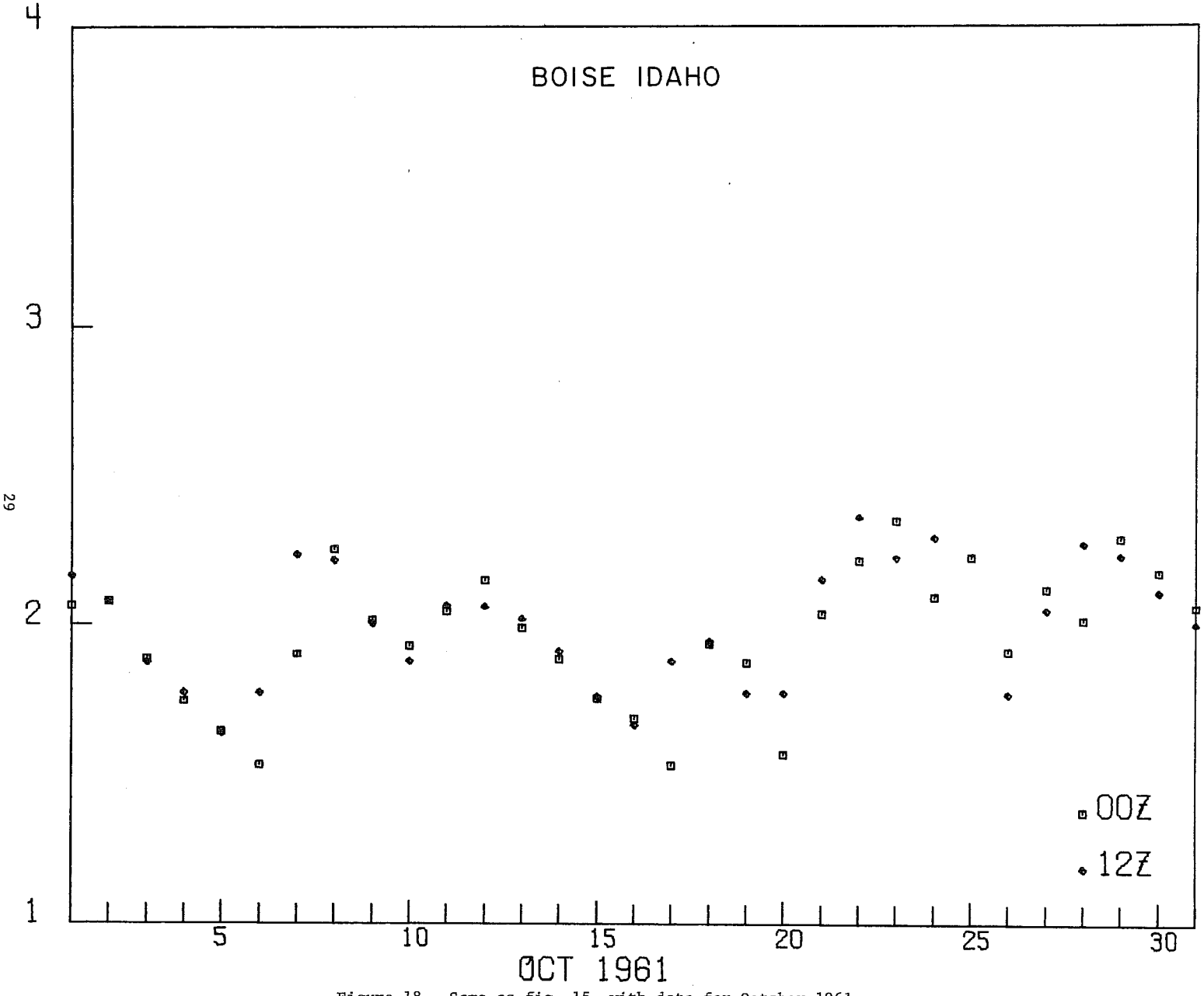

Figure 18. Same as fig. 15, with data for October 1961.

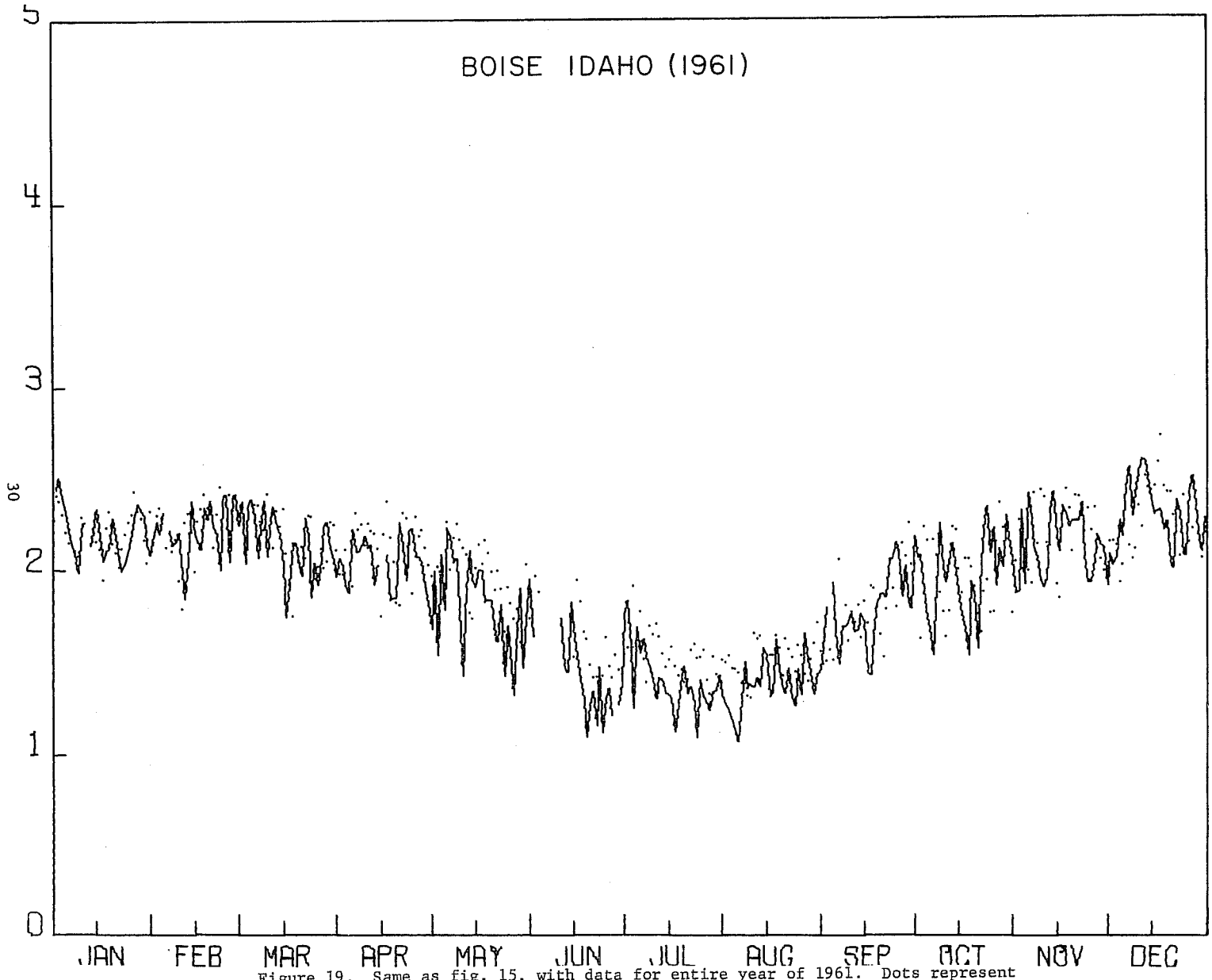

Figure 19. Same as fig. 15, with data for entire year of 1961. Dots represent 00Z observations; continuous line shows 12Z observations.

of August 4, 1961, when it reached 110°F in Boise, and 2847 m (ASL) on the morning of January 11, 1963, when it reached -5°F at Boise - an extreme range of 1783 m in 3 years. An extreme range of 1051 m was observed in a single month, June 1962. A number of times there were changes of 500 m or more in 24 hours. Flight altitudes, high enough to allow successful flights with preinflated tetroons with minimum equilibrium altitudes of 150 m, should therefore be about 700 m above ground. This would mean that flights during cold periods may have equilibrium flight altitudes of 1200 m.

If a method were invented to automatically set the ballast at the sound of the alarm, just before the tetroon release, then (7) where L_{ni} is now known could be used to determine the flight altitude as affected by $\frac{\partial \rho_a}{\partial Z}$. Table 7 shows the analysis of the 900-mb to 850-mb layer over Boise for 1961-1963. The least negative value for this period was -0.631×10^{-7} (g cm^{-3}) (m^{-1}) on July 23, 1963, when the temperature decrease with altitude was 7.5°C in the 900- to 850- mb layer. The greatest negative value was -2.46×10^{-7} (g cm^{-3}) (m^{-1}) on January 31, 1963, when the inversion was 11.1°C in the layer. If these values were inserted in (7), with L_{ni} = 10 m and $V = 3.2 \times 10^5$ cm^3 for a 42-inch tetroon, the flight altitude for the hot summer afternoon would be very close to 500 m, and for the cold winter morning it would be close to 125 m.

In conclusion, we should recognize that the mean flight altitudes of tetroons preinflated to fly at some given density level will vary greatly making such tetroons highly undesirable for plume transport simulation. If the ballast could be automatically adjusted to give a predetermined free lift at release, the equilibrium flight altitude variations would be only a few hundred meters and would allow the tetroon to serve as a simulator of the plume transport. Other considerations will be studied to see what time (days, week, etc.) will be needed to manually check the balloon's ballast for proper flight altitude.

2.4 A Statistical Technique for Surface Wind Forecasting

An objective forecast technique for surface winds has been developed (ESSA Tech. Memo. ERLTM-ARL 9, 1968) which shows considerable promise for verifications on the second day of a 36-hour forecast. Regression estimation of event probabilities (REEP) is used with nine categories of maximum afternoon surface winds for the predictand (Miller, 1964) and objectively derived upper air map types for the predictors (Lund, 1963).

2.4.1 Predictand and Predictors

All observations of the maximum average hourly wind speed at the NRTS Central Facilities between 1000 and 1900 MST in April and May 1962 through 1967, the only map data available, were plotted on polar coordinate paper to determine a reasonable division of predictand categories. The resulting categories are shown in figure 20. The great majority of winds were SW to S, and nearly all others were NNW to NE. Since all observations in category

Table 7. Analysis of Density Gradient $(\frac{\partial \rho_a}{\partial z})$ Between 900 and 850 mb Over Boise, Idaho. Units are x 10^{-7} (g cm^{-3}) (m^{-1}); values are negative

		0000Z			1200Z		
Year	Month	Mean	Max.	Min.	Mean	Max.	Min.
1961	1	1.24	1.79	0.95	1.39	1.80	1.08
	2	1.04	1.24	0.84	1.14	1.29	1.00
	3	0.94	1.14	0.74	1.18	1.54	1.03
	4	0.91	0.98	0.80	1.23	1.54	1.04
	5	0.85	0.96	0.74	1.22	1.69	0.95
	6	0.82	0.94	0.70	1.29	1.55	0.93
	7	0.79	0.96	0.65	1.30	1.68	0.92
	8	0.82	1.13	0.65	1.17	1.58	0.86
	9	0.89	1.10	0.77	1.20	1.49	0.97
	10	1.00	1.27	0.87	1.27	1.67	1.00
	11	1.08	1.28	0.95	1.29	1.73	1.06
	12	1.17	1.58	0.96	1.26	1.69	1.03
1962	1	1.43	2.22	1.02	1.53	2.19	1.12
	2	1.32	2.32	0.94	1.46	2.32	1.01
	3	0.98	1.25	0.85	1.24	1.60	1.10
	4	0.89	1.17	0.77	1.22	1.66	0.95
	5	0.84	1.04	0.74	1.24	1.60	0.95
	6	0.83	0.93	0.73	1.28	1.59	0.98
	7	0.82	1.00	0.73	1.26	1.52	1.02
	8	0.82	0.97	0.72	1.20	1.53	0.95
	9	0.87	1.14	0.74	1.22	1.62	0.97
	10	0.98	1.31	0.73	1.28	1.61	0.96
	11	1.09	1.58	0.94	1.28	1.59	1.07
	12	1.19	1.62	0.99	1.33	1.73	0.97
1963	1	1.23	1.85	0.95	1.51	2.46	1.11
	2	1.01	1.43	0.83	1.26	1.74	0.96
	3	0.91	1.08	0.74	1.17	1.49	1.01
	4	0.91	1.18	0.77	1.13	1.37	1.01
	5	0.85	1.02	0.70	1.18	1.48	0.94
	6	0.91	1.09	0.73	1.15	1.44	0.96
	7	0.78	0.91	0.63	1.26	1.50	0.94
	8	0.79	0.90	0.65	1.27	1.54	0.95
	9	0.86	1.71	0.66	1.11	1.50	0.91
	10	0.91	1.18	0.77	1.18	1.55	1.00
	11	1.04	1.41	0.85	1.20	1.67	0.87
	12	1.39	1.95	0.99	1.55	1.92	1.10

3 were from 140° to 195°, this category should be regarded as S to SE winds. After missing predictor data were considered, only 4 percent of observations fell into category 4 and 4 percent into category 9, which makes it nearly impossible to forecast these categories.

The predictors for a given experiment were map types derived at one of three levels of the troposphere, 850 mb, 700 mb, and 500 mb. Three experiments were run to determine from which level the best results might be expected. After the map types were derived for a level, all days in the sample for April and May 1962 through 1967 were correlated to these types to determine which ones depicted each sample day. In some cases there were

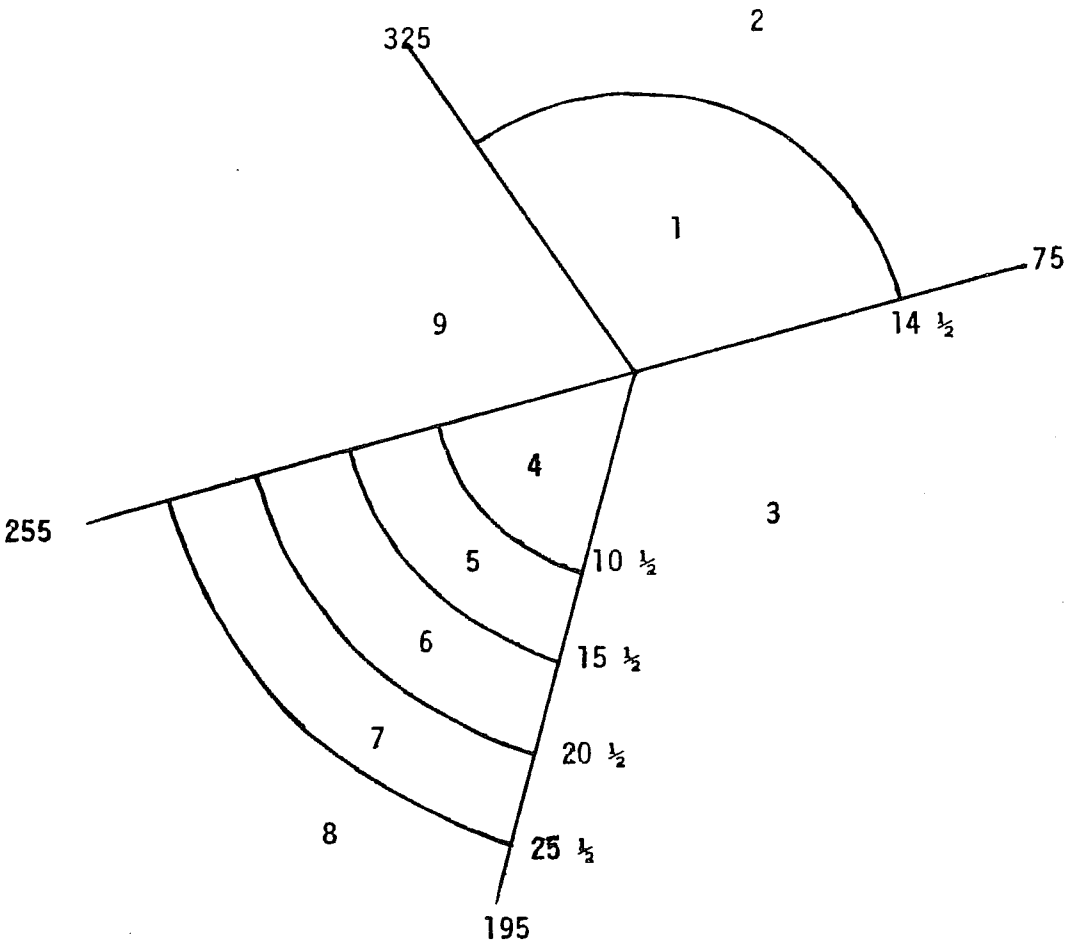

Figure 20. Direction (degrees) and speed (miles per hour) boundaries of the nine wind categories used as predictands in the REEP prediction model.

no significantly correlated map types, in other cases there was one or even as many as five. All simple and combination map types occurring 10 times or more over the entire sample were used as predictors. Only a few combinations of three types and no four-type combinations occurred in significant numbers. Table 8 gives the number of predictors for each experiment, as well as the number of cases from the sample that were not significantly correlated to any map type. The large number of no-type cases at the 850-mb level suggests that it is impractical to use 850-mb map type predictors unless they give greatly superior results when compared with the 700-mb and 500-mb forecasts.

2.4.2 Forecast Verification

Subjective forecasts issued at 0900 MST were available for comparison only for 1965 through 1967 and were made only 5 days per week. Because of a few missing maps from the map-typing sample, the forecast sample was not the same for each of the three experiments: 109 cases for the 850-mb experiment, 116 cases for the 700-mb experiment, and 113 cases for the 500-mb experiment for comparison with second day forecasts. Because subjective forecasts for the first day (0-12 hours) were better than the objective, no further first-forecast-period comparisons are made in this report.

REEP forecasts were verified under the assumption the highest probability category was the forecast category, and the assumed forecast was according to the assignments of table 9. Subjective forecasts were verified on the assumption of a speed that was the midpoint of a forecast speed range. The subjective forecast directions naturally fell into the derived categories. The error between forecast and observed wind vectors was determined by the magnitude of the vector difference.

The average error of a forecast deviated little for a given pair of forecast and observed categories and was assigned a B- value according to the average error for the pair given in table 10. A resulting array of B-values is shown in table 11 for computing a score similar to the Brier-Allen score:

$$\bar{S} = \frac{1}{n} \sum_{i=1}^{n} B_i^2 \quad . \tag{8}$$

Table 12 summarizes the $\bar{S}$ scores for the three experiments. The first column is a summary for all cases. Unfortunately, the REEP forecast on days when there is no assigned map type is necessarily equal to the constant terms of the equations. The second column assumes no REEP forecast is made on no-map-type days, since a high percentage of such days results in large vector errors.

The 850-mb forecasts were not considered for operational use for two reasons: (1) the 850-mb forecasts were inferior to the 700-mb and 500-mb forecasts, and (2) there was a much larger number of no-map-type days at 850 mb than at the other two levels. The 700-mb forecasts will be used because they are superior to the 500-mb forecasts. It is significant that REEP 700-mb map type forecasts had only half as many incorrect forecasts as the subjective

Table 8. Number of Basic Map Types, Number of Combination Map Types, and Number of Sample Days not Correlated at >0.80 to Any Map Type

Experiment	Basic Types	Combination Types	No-Type Cases
850 mb	15	10	102
700 mb	13	19	60
500 mb	17	36	48

Table 9. Assumed Values of Forecast Direction and Speed for a Given Forecast Category

Category	Assumed Forecast	Category	Assumed Forecast
1	20^{o} 11 mph	7	230^{o} 23 mph
2	20^{o} 17 mph	8	230^{o} 28 mph
3	170^{o} and speed as forecast by highest probability from groups 4 - 8.	9	270^{o} and speed as forecast by highest probability in groups 4 - 8 or 310^{o} and speed as forecast by highest probability between groups 1 and 2, depending on whether the highest probability (aside from group 3) was in groups 1 or 2, or in groups 4 - 8.
4	230^{o} 8mph		
5	230^{o} 13 mph		
6	230^{o} 18 mph		

Table 10. The Assignment of B-Values According to Mean Errors Between Forecast and Observed Wind Categories

	mph									
Average Error	0-2	3-6	7-10	11-14	15-18	19-22	23-26	27-30	31-34	34-38	$\geq$39
B-Value	0	.1	.2	.3	.4	.5	.6	.7	.8	.9	1.0

Table 11. The Values of B to be Used in the Skill Score $(\bar{S}) = \frac{1}{n} \sum B^2$

Category	Category 1	2	3	4	5	6	7	8	9
1	0	.1	.4	.4	.5	.6	.7	.8	.4
2		.0	.7	.6	.7	.7	.9	1.0	.5
3			.1	.3	.3	.3	.3	.4	.6
4				0	0	.2	.3	.5	.2
5					0	.1	.2	.3	.2
6						0	.1	.2	.3
7							0	.1	.4
8								0	.5
9									.1

The matrix is symmetric; use row (column) for forecast category and column (row) for observed category.

Table 12. Comparison of $\bar{S}$ Scores Between Objective and Subjective Forecasts of CFA Maximum Afternoon Winds 24 to 36 Hours From Forecast Time.

Experiment	Cases	S	Incorrect Forecasts*	Cases	$\bar{S}$	Incorrect Forecasts
Subjective	109	.089	19	71	.046	7
REEP - 850 mb	109	.144	27	71	.090	10
Subjective	116	.099	25	97	.091	21
REEP - 700 mb	116	.115	23	97	.073	10
Subjective	113	.100	25	98	.088	20
REEP - 500 mb	113	.122	26	98	.090	16

*An incorrect forecast is a B-value of 0.5 or more.

forecaster, namely one out of 10 against one out of five, while the 500-mb forecasts by REEP made only a 20 percent improvement. The improvement of second-day wind forecasting by the objective technique over the subjective forecaster is sufficiently great to merit its use, and to justify studies of other seasons and for larger data samples.

2.5 Hemispheric Dispersion

The objective of this project is to study the dispersive nature of wave motion over the Northern Hemisphere for wavelengths longer than 500 miles. The current preliminary phase of the study is limited to the dispersion of hypothetical particles carried by winds on an isobaric surface, 500 mb, and to the effect on the dispersion of various interpolation schemes applied to available data.

The work reported here is primarily the check-out phase of the trajectory construction and dispersion calculations. The data used are the National Meteorological Center (NMC) 12-hourly 500-mb stream function values defined on the NMC grid for December 1963 and January 1964. The trajectory was constructed from stream function-derived winds and with an iterative scheme for advecting the particles. The schemes validity was tested by constructing 6-day trajectories, on a stationary map, for eight particles equally spaced around $50^{o}N$ and by comparing the trajectories with the streamline analysis for the map. A 2-hour advecting step was used. The trajectories and stationary streamline agreed quite well even for closed loops as small as 500 miles in diameter. However, trajectories constructed from a stream function pattern changing with time occasionally showed much sharper changes in direction. An optimum time interval for the advection process will have to be determined.

Initially, two methods for interpolating the stream function fields between the 12-hourly observations were tested. The first method consisted of simply holding each map fixed for a 12-hour period, then changing abruptly to the next map. The second method allowed the stream function values at each grid point to change linearly from one map to the next. A four-point polynomial technique and a four-point spline function are being incorporated into the program for testing. Only half of the plots of the eight trajectories for each scheme differed severely. As might be expected, these traversed the portion of the hemisphere that had the more significant changes in flow pattern during the 6-day period. The trajectories constructed with the linear time interpolation were, of course, much smoother,but the large difference in final position of some of the particles indicated that more sophisticated interpolation techniques should at least be tested.

The quantity of interest is the latitudinal dispersion of the particles, D_L, which is defined as

$$D_L(t) = \frac{1}{N} \sum_{i=1}^{N} \left[\varphi_i(t) - \varphi_\gamma\right) \frac{\pi}{180} R_e\Big]^2 , \qquad (9)$$

where t is time, N is the number of particles released from positions equally spaced around the latitude circle, φ_i (t) is the latitude of particle number i, φ_γ is the release latitude, and R_e is the radius of the earth. Besides the natural phenomena that govern the behavior of D_L (t), other factors are introduced in the computation of the quantity. One, which we have already discussed, is the validity of the hypothetical trajectories, and another is the size of the sample of particles released. A comparison of the D_L (t) functions as computed with the two time interpolation techniques for a 72-particle sample over a 6-day period in December 1963 is shown in figure 21. The method in which stationary maps for 12 hours at a time are used shows about 35 percent more dispersion at the end of the period. Also, D_L (t) for the linear interpolation method shows a negative trend during the last 3 days of the period. This would indicate that the more crude interpolation technique introduces spurious dispersion.

To examine the representativeness of a 27-particle sample (5^o of longitude), D_L (t) for sample sizes of 8 and 36 were computed for the same 6-day period and are shown in figure 22. Since the curves for the 72- and 36-particle samples are quite similar, a 72-particle sample is assumed adequate.

Note in both figures 21 and 22 sudden drops in the values of D_L (t). These are caused by the loss of a particle from the data field, which covers the Northern Hemisphere north of 20^oN. It is apparent from figure 22 that the procedure of simply dropping the particle from the sample is unsatisfactory, and other methods are now being considered and tested. Once the most satisfactory one is selected, D_L (t) may be computed by more sophisticated time interpolation techniques and for much longer time periods.

2.6 Deposition and Depletion Studies

During this semiannual period, two field releases for deposition study were conducted at the Experimental Dairy Farm (EDF). The first was a release of elemental radioiodine $^{131}I_2$ over Trudan grass on August 15; the second was a release of radioactive sulfur in the form of $^{35}SO_2$ over an alfalfa plot on September 18. During both releases, wind velocity and temperature profiles from 1 to 4 m at EDF and from 1 to 61 m at Test Grid III were measured to document the meteorological boundary layer conditions. The median deposition velocities were 9 cm/sec for $^{131}I_2$ on Trudan grass and 2 cm/sec for $^{35}SO_2$ on alfalfa. The high deposition velocity obtained for $^{131}I_2$ on Trudan grass agrees with the relationship found previously between deposition velocity normalized by grass density and surface boundary layer transport velocity, $u^{*2}/\bar{u}$ (Markee, 1967). Future field tests are planned for summer 1969,

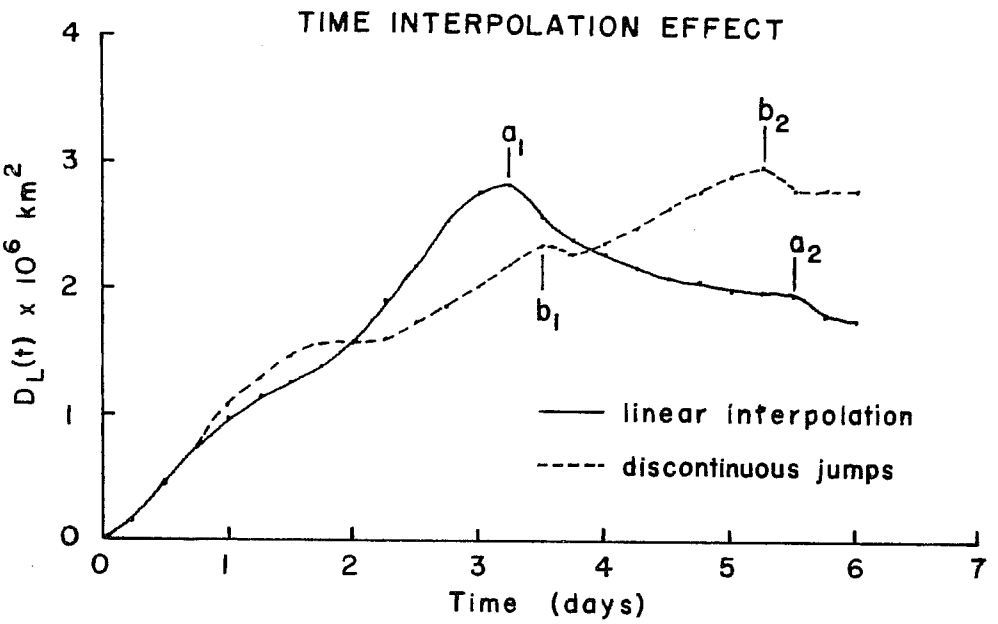

Figure 21. Hemispheric dispersion, $D_L(t)$, of 72 particles released from equally spaced positions around latitude 50° N on the 500-mb surface. At points a_1 and b_1 one particle was lost from the sample. At points a_2 and b_2 a second particle was lost from the sample.

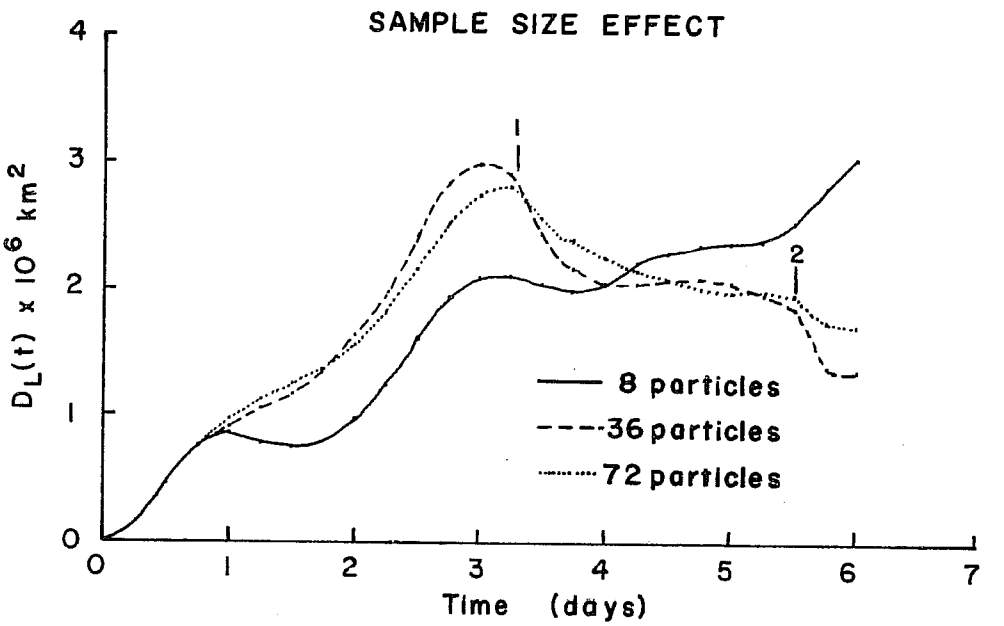

Figure 22. Hemispheric dispersion, $D_L(t)$, of samples of various sizes released from equally spaced positions around latitude 50° N on the 500-mb surface. At point 1 in both the 36- and 72-particle samples, one particle was lost. At point 2, a second particle was lost from each of the samples.

during which turbulence in grass canopies and distribution of deposition on the grass will be measured.

A preliminary series of 16 $^{131}I_2$ tests of deposition on activated carbon plates suspended in the CERTLE environmental chamber was completed. Ten-inch square and 5 x 10-inch plates covered on both sides with 2 x 2-inch and 1-2/3 x 2-inch pieces of activated carbon filter paper were used to measure variations in total deposition and distribution of deposition on the plate faces with plate orientation of 90^{o}, 60^{o}, 30^{o}, and 0^{o} with respect to the floor of the chamber. These tests were not too successful because deposition and reentrainment of iodine deposited on the chamber walls prevented accurate determination of the amount and spatial distribution of the effluent. Also, a uniform, horizontal, and consistent cross-sectional wind velocity was hard to maintain because of the very slow air flow through the chamber (average linear velocity: 20 cm/sec). Despite these difficulties the measurements indicated that:

1. With the flow parallel to the plate (0^{o} incidence), deposition is inversely proportional to the fourth root of distance from the leading edge of the plate. This agrees with the Prandtl formulation for skin friction drag and development of the boundary layer over a flat plate in turbulent flow.

2. For all plate orientations, deposition was greater ($\sim$12%) on the edges than in the center of the plate. This indicates that edge effects may be important in the assessment of deposition.

This study will be pursued further in the new environmental chamber where wind velocity and turbulence can be controlled.

2.7 Turbulence Analysis

A computer program has been constructed for computing energy spectra by the fast Fourier transform technique. Two algorithms for computing the complex Fourier coefficient are available: one, reported by Foreman (1966), does not require the inversion of the order of the binary bits for the subscripts of the coefficients; the other is a routine based on the original Cooley and Tukey (1965) algorithm, which requires inversion of the order of the bits but about 35 percent less computer storage space than the first algorithm. These programs, instead of the version used by the ARL office in Silver Spring, Md. (ESSA Tech. Memo. ERLTM-ARL 5, 1968) were used because of the difficulty in converting local computers. Some of the techniques for preprocessing the data were incorporated into this program, as well as an option by which linear trends my be removed from the data.

A band-averaging option has also been included for smoothing the spectra. All that need be specified is the frequency at which the averaging is to start and the initial number of points in the band. The number of points is doubled at each succeeding higher octave. A plot routine that provides the option of plotting the spectral results in semilog or log-log form has also been added.

A program has been constructed that computes the correlation function, based on the fast Fourier transform, first by a transformation of the original data, then by an inverse transformation on the conjugate products of the complex coefficients. This procedure seems to be considerably more efficient than the direct computation of correlation coefficients for data strings longer than a few hundred points.

3.0 REFERENCES

Cooley, J. W., and J. W. Tukey (1965), An algorithm for the machine calculation of complex Fourier series. Math. Computation 19, 297-301.

Dickson, C. R ., ed. (1967), Meteorology for the loss of fluid test reactor, U. S . Atomic Energy Commission Report, IDO-12059, 55 pp.

ESSA Tech. Memo. ERLTM-ARL 5 (1968), Atmospheric transport and diffusion in the planetary boundary layer, Air Resources Laboratories Semiannual Research Program Review for the Division of Reactor Development and Technology, USAEC, 60 pp.

ESSA Tech. Memo. ERLTM-ARL 9 (1968), Atmospheric transport and diffusion in the planetary boundary layer, Air Resources Laboratories Semiannual Research Program Review for the Division of Reactor Development and Technology, USAEC, 60 pp.

Foreman, M. L. (1966), Fast Fourier transform technique and its application to Fourier spectroscopy, J. Opt. Soc. Am. 19, 987-979.

Islitzer, N. F., and R. K. Dumbauld (1963), Atmospheric diffusion-deposition studies over flat terrain, Int. J. Air Water Pollution 7, 999-1022.

Lumley, J. L. and H. A. Panofsky (1964), The Structure of the Atmosphere (John Wiley & Sons, New York) 239 pp.

Lund, A. (1963), Map-Pattern classification by statistical methods, J. Appl. Meteorol. 2, No 1, 56-65.

Markee, E. H., Jr. (1967), Turbulent transfer characteristics of radioiodine effluents from air to grass, AECL-2787, Proc. USAEC Meteorol. Inform. Meeting, Chalk River Nuclear Laboratories, AECL, Chalk River, Ontario, Canada, 589-599.

Miller, G. (1964), Regression estimation of event probabilities, USWB Contract Cwb-10704, Tech. Rept. No. 1, Travelers Research Center, Hartford, Conn., 152 pp.

Panofsky, H. A., and B. Prasad (1965), Similarity theories and diffusion, Intern. J. Air Water Pollution 9, 419-430.

Shepard, D. (1968), A two dimensional interpolation function for irregularly-spaced data, Proc. 1968 ACM Natl. Conf., (Branden Systems Press, Princeton, New Jersey.)

4.0 REVIEW OF REACTOR SAFETY ANALYSIS REPORTS

The Air Resources Laboratories in Silver Spring, Maryland, and the Field Office in Idaho have continued to take an active part in the review of reactor safety analysis reports as well as consultations with regard to the preparation of the reports. In addition, written comments have been prepared for the Division of Reactor Licensing through the Division of Reactor Development and Technology as follows:

1. Calvert Cliffs Nuclear Power Plants Units 1 and 2, Baltimore Gas and Electric Company Preliminary Safety Analysis Report, Amendment No. 2, dated June 28, 1968.

2. Edwin I. Hatch Nuclear Power Plant, Georgia Power Company Preliminary Safety Analysis Report, Volumes I, II, III and IV, dated May 1968.

3. Shoreham Nuclear Power Station, Long Island Lighting Company Preliminary Safety Analysis Report, Volumes I, II, III and IV, dated June 1968.

4. Brunswick Steam Electric Plant, Carolina Power and Light Company Preliminary Safety Analysis Report, Volumes I, II and III, dated July 31, 1968.

5. Donald C. Cook Nuclear Plant, Indiana and Michigan Electric Company Preliminary Safety Analysis Report, Amendment Letter dated, September 30, 1966.

6. Quad-Cities Station, Units 1 and 2, Commonwealth Edison Company and Iowa-Illinois Gas and Electric Company Safety Analysis Report, Volumes I, II and III, dated August 30, 1968.

7. Southwest Experimental Fast Oxide Reactor Facility Description and Safety Analysis Report, Supplement 19, Appendix I, dated August 1968.

8. Indian Point Nuclear Generating Unit No. 2,Consolidated Edison Company of New York, Inc. Final Facility Description and Safety Analysis Report, Volumes I, II, III and IV, dated October 15, 1968.

9. Dresden Nuclear Power Station, Units 2 and 3, Commonwealth Edison Company Safety Analysis Report, Volumes I and II, dated November 17, 1967, and Appendix A dated August 30, 1968.

10. Calvert Cliffs Nuclear Power Plants, Units 1 and 2, Baltimore Gas and Electric Company Preliminary Safety Analysis Report, Amendment No. 4, Supplement 2, dated November 7, 1968.

11. Sequoyah Nuclear Plant, Tennessee Valley Authority Preliminary Safety Analysis Report, Volumes I, II, and III dated October 15, 1968.

5.0 PUBLICATIONS

1. Angell, J. K., D. H. Pack, and C. R. Dickson, "A Lagrangian study of helical circulations in the planetary boundary layer," J. Atmospheric Sci. 25, No. 5, 707-717, September 1968.

2. Dickson, C. R. and J. K. Angell, "Eddy velocities in the planetary boundary layer as obtained from tetroon flights at Idaho Falls, "J. Appl. Meteorol. 7, No. 6, 986-993, December 1968.

3. Kao, S. K. and L. L. Wendell, "Some characteristics of relative dispersion in the atmosphere's boundary layer," Atmospheric Environ. 2, No. 4, 397-407, July 1968.

4. Slade, D. H. (Editor), "Meteorology and atomic energy 1968," USAEC report TID-24190, 445 pp., July 1968.

6.0 LABORATORY PERSONNEL

Silver Spring, Md.

Abram B. Bernstein, meteorologist, went on leave-without-pay status on Oct. 9, 1968, in order to complete the fall-winter semester of graduate study at the University of Washington, Seattle, Washington.

Idaho Falls, Idaho

Judith Zavala, temporary clerical help, terminated July 13, 1968, to accept permanent employment with the Dept. of Interior.

Delbert Sharp, meteorological technician, rejoined the staff Aug. 5, 1968, after a 16-month tour of duty in Central America with the AEC-sponsored Interoceanic Canal Project.

Annette Barnes, summer physical science aid, terminated on Aug. 30, 1968, to return to her university studies.

William Wiser, summer working aid (YOC), terminated on Sept. 20, 1968, to begin his university studies.

Professor Don Dickson, University of Utah, Salt Lake City, completed his micrometeorological data gathering program at the NRTS and returned to the university on September 12, 1968, to complete his research. His summer fellowship at NRTS was supported by the AEC through the Associated Western Universities.

Earl Markee, meteorologist, returned to his university training assignment for the period Oct. 23 to Dec. 16, 1968, to complete the last of four quarters of ESSA-sponsored training at the University of Utah.

Kae Sidle, mathematical analyst, entered on duty November 19, 1968.